Statistical modeling of the gas-liquid interface using geometrical variables: toward a unified description of the disperse and separated phase flows

Mohamed Essadki, Florence Drui, Stéphane de Chaisemartin, Adam Larat, Thibault Ménard, Marc Massot

Statistical modeling of the gas-liquid interface using geometrical variables: toward a unified description of the disperse and separated phase flows

ESSADKI Mohamed[a,b,c], DRUI Florence[b,c,e], de CHAISEMARTIN Stéphane[a], LARAT Adam[b,c,g], MÉNARD Thibault[f], MASSOT Marc[b,c,h,*]

[a] *IFP Energies Nouvelles, 1-4 Avenue du Bois Préau, 92852 Rueil-Malmaison, France*
[b] *EM2C, UPR 288 - CNRS, CentraleSupélec, Université Paris-Saclay, 3, rue Joliot-Curie 91190 Gif-sur-Yvette France*
[c] *Fédération de Mathématiques de CentraleSupélec, FR 3487 - CNRS, CentraleSupélec, Université Paris-Saclay, 8-10, rue Joliot-Curie 91190 Gif-sur-Yvette, France*
[d] *Maison de la Simulation, USR 3441, Digiteo Labs, bât. 565, PC 190, CEA Saclay, 91191 Gif-sur-Yvette, France*
[e] *CEA/DEN/DANS/DM2S/SEMT/DYN - CEA Saclay, 91191 Gif-sur-Yvette, France*
[f] *CORIA, UMR 6614 - Normandie Université, CNRS, Université et INSA de Rouen, Site Universitaire du Madrillet, BP 12, 76801 Saint-Etienne-du-Rouvray cedex, France*
[g] *Univ. Grenoble Alpes, CNRS, Grenoble INP, LJK, 38000 Grenoble, France*
[h] *CMAP, UMR 7641 - CNRS, Ecole Polytechnique, Institut Polytechnique de Paris, 91128 Palaiseau, France*

Abstract

In this work, we investigate an original strategy in order to derive a statistical modeling of the interface in gas-liquid two-phase flows through geometrical variables. The contribution is two-fold. First it participates in the theoretical design of a unified reduced-order model for the description of two regimes: a disperse phase in a carrier fluid and two separated phases. The first idea is to propose a statistical description of the interface relying on geometrical properties, such as the mean and Gauss curvatures, and to define an associated Surface Density Function (SDF). The second main idea consists in using such a formalism in the disperse case, where a clear link is proposed between local statistics of the interface and the statistics of countable objects, such as a number density function. To this end we make essential the use of topological invariants in geometry through the Gauss-Bonnet formula. This strategy strictly includes the works conducted on sprays of spherical droplets, but it also yields a statistical treatment of populations of non-spherical objects, such as ligaments, as long as they are homeomorphic to a sphere. Second, we propose an original statistical post-processing of DNS data of interfacial flows. Starting from the proposed theoretical approach, we identify a kernel for the spatial averaging of geometrical quantities which preserves the topological invariants. Coupled to a new algorithm for the evaluation of the surface and its curvatures, that also preserves these invariants, we analyze two sets of DNS results obtained with the ARCHER code from CORIA, with and without topological changes, and assess the approach. Indeed, this procedure allows us to transform the interfacial information provided by a Level-Set function into a number distribution of a collection of objects in the proper geometrical phase space.

[*] Corresponding author - marc.massot@polytechnique.edu

Keywords: disperse/separated phases, gas-liquid interface, moments method, Gauss-Bonnet formula, computational geometry, surface and number density function.
2010 MSC: 76T10, 65D99, 53A17, 76A99, 35Q35

1. Introduction

Nowadays, direct fuel injection systems are widely used in automotive engines to better atomize and mix the fuel with the air, in order to improve the combustion, reduce pollutant emissions and save fuel. The design of new and efficient injectors need to be assisted by predictive numerical simulations to test new configurations, understand the various physical mechanisms involved in this complex problem and at the same time, at a reduced price compared to experiments. Near the nozzle outlet, of diameter less than $1mm$, the fuel is a bulk liquid phase, separated from the gaseous phase. In this region, the two-phase flow is denoted *separated phases*. After primary atomization, the fuel is desintegrated into a polydisperse spray. Indeed, the large drops can undergo a secondary breakup leading to a cloud of very small disperse droplets of size around $1 - 10\,\mu m$, called the *disperse phase*. The major challenges faced by the modeling of fuel injection are three-fold: the strong multi-scale feature of the considered problem, the coexistence of two specific two-phase regimes (the *separated* and the *disperse* regimes) and the entanglement between the first two points within the *transitional* regime.

In Direct Numerical Simulation (DNS), each phase dynamics is resolved through monophasic Navier-Stokes equations while the gas-liquid interface is determined using interface capturing methods (VOF, level-set or a combination of both methods) [1, 2, 3, 4] or interface tracking methods, as initiated in [5]. DNS codes, such as the ARCHER code [4], may be used for simulations of academic and some simple injection configurations. The results of these simulations help to better understand the phenomena, since accurate information on detailed physics is sometimes hard to extract from experimental measurements [6, 7, 8, 9, 10]. However, configurations at large Reynolds number, that characterizes the turbulent regime of the flow, or at large Weber number, related to the stability of the interface, may be extremely costly from a numerical point of view. Besides, one has to be very careful in terms of refining the mesh in order to reproduce the proper physics, since the range of scales involved in the process is not bounded from below as in turbulence [11, 12]. Therefore, DNS is of great interest in academic research, and, even if some industrial and realistic configurations are amenable to DNS, most of the time, it is too costly or beyond reach for current industrial use.

Reduced-order models intend to avoid the simulation of the smallest scales of the configuration by providing a description and evolution laws only for some quantities of interest, such as for example the volume fraction of the phases in mixture zones or the area density of the two-phase interface. So far, however, these models inherently depend on the two-phase flow regime: the separated or the disperse phase regimes. Building up a multi-scale and accurate model with the capacity of resolving the whole injection process is a challenging task, that can be addressed either by coupling models

associated with the two main flow classes, namely the disperse and separated phase flows, or by developing a unified approach.

The reduced-order models for disperse phase flows usually adopt a statistical approach. They rely on a number density function (NDF), that satisfies a generalized population balance equation (GPBE), also known as the Williams-Boltzmann Equation (WBE) [13]. The phase space variables of the NDF can include different physical properties of the disperse particles (droplets in the case of atomization) such as velocity, size and temperature. However, the large phase-space dimension makes the deterministic resolution of the WBE quickly unaffordable. Then, multiple approaches have been developed. First, one can use a Lagrangian Monte-Carlo approach to estimate the NDF [14]. Even though this approach can be considered as the most accurate for solving WBE, it still suffers from many drawbacks: the need for a high number of numerical particles to ensure the statistical convergence, the requirement of complex load balancing algorithms for parallel computations or the difficulty of coupling with the gaseous phase, which is most of the time solved in an Eulerian framework. Second, one can derive Eulerian moment models from the WBE. With these models, the NDF is not directly solved, but one solves for a finite set of its moments. Then, a most likely NDF can be reconstructed from the finite number of moments. For mathematical and modeling reasons, we work with a compact size interval (as in [15] and references therein) and the moment problem is thus called the Hausdorff moment problem [16]. Among the properties of a disperse phase, the size-distribution of the droplets has a major impact on the results of the combustion simulations [17, 18]. Currently, in the context of Eulerian moment methods, this distribution can be accounted for in three ways:

A. multi-fluid models, where the size phase space is discretized into size bins, called *sections*. Then moments up to order two can be used in each section [19, 20],
B. quadrature-moment methods such as QMOM, DQMOM or EQMOM [21, 22], consider the NDF as a sum of Dirac-delta functions, potentially extended to kernels,
C. high order moments with continuous reconstruction developed in [23, 24, 15]. At each step, a continuous NDF maximizing the Shannon entropy is reconstructed from the high order moments [25], with a complete coverage of the whole moment space.

Using high order moments with continuous reconstruction through entropy maximization avoids the use of several sections, that are computationally more expensive [26]. Moreover, the continuous reconstruction allows a more accurate and consistent evaluation of the evaporation flux, compared to the discontinuous approach used in the quadrature-moment methods, as well as a comprehensive description of the moment space. In the current work, we adopt this approach.

Among the different approaches that may be used in separated-phase configurations, let us mention the interface capturing methods based on the resolution of a two-fluid or mixture model, resulting in a system of PDEs as in [27, 28, 29]. These equations may be derived through an averaging procedure [30, 31], or by using a variational principle [32, 33]. In both cases, they stand for a spatial-, temporal- or ensemble-averaged two-phase flow, where one or both phases can be present at any given location,

according to the values of a characteristic function, that is generally the volume fraction of one of the phases. Traditionally, these models provide little information about the sub-scale interfacial structures. Recent works, as in [33], have shown that they can be enriched with further sub-scale physics. Yet, such models are far from the ability to deal with polydispersity, in the way kinetic models do. From a numerical point of view, two-fluid models are used for simulations of separated phases and interfacial configurations, for which the exact location of the interface is not reconstructed, but lies in a mixture zone due to numerical approximation. Although the numerical diffusion can be reduced by using more accurate numerical schemes, the spreading of the interface is still a main bottleneck of these methods for the simulation of atomization.

Recent works have been devoted to the numerical coupling between separated phases and disperse phase approaches. Among them, LeTouze et al [34] proposed to couple a diffuse interface model for separated phases with a multi-fluid model for the disperse phase. Up to now, the exchange terms between both models depend on the configuration of the atomization and cannot predict the distribution in size of the disperse droplets. One can also mention the Eulerian-Lagrangian Spray Atomization (ELSA) [35, 36, 6] technique, where a two-fluid model is enhanced with an equation for the expected surface area density in the dense zones. This model is then coupled with a Lagrangian approach for the simulation of the disperse phase in the dilute zones. In [37], the same set of equations is used with a differentiation between the variables describing the disperse and separated phases. Two additional equations on the expected density area are also used: one for the separated phases and one for the disperse phase. So far, these approaches do not provide a unified description of the whole atomization process (from the separated phase to the spray of droplets) and fail in providing an accurate description of the polydispersion for the disperse phase. Indeed, in the works presented above, the description of the gas-liquid interface geometry relies on one or two variables only, that are the volume fraction and the expected surface area density. This information is not sufficient to reconstruct a NDF of a polydisperse spray.

The idea of the present work is to study the possibility of describing gas-liquid interfaces by using some additional geometrical information, such as the mean and Gauss curvatures, for which evolution equations have been derived in [38]. Moreover, the coupling with Eulerian models for sprays is considered through a statistical description of the interface. First, inspired by the pioneering works of [39] for the description of the dynamics of flames, we define a Surface Density Function (SDF) within a different phase space: in our work, it is composed of the mean and Gauss curvatures and the interfacial velocity. The key issue is to make the link between the statistics of a local description of the interface through geometrical variables, such as curvatures, and the statistical description of isolated objects through a number density function in the appropriate phase space. A discrete formalism of the SDF is then proposed to describe disperse phase flows. In this case, the geometrical quantities are averaged on the surface of isolated droplets or bubbles. We show that this new formalism can be related to the high-order moment model proposed in [15, 40] for sprays of spherical droplets. Indeed, by considering fractional moments of a NDF, this model uses the same geometrical quantities to describe the polydispersity of the droplets. Going forward into a full generalization of the interface description, we consider spatially averaged SDF (ASDF), with an averaging kernel bounded to a small region around the interface. This

spatial average is applied to each separated realization, before an ensemble average is applied. When performed in a consistent way, this process preserves some necessary topological properties of the gas-liquid interface description. This leads us to the definition of a generalized NDF (GNDF), which can be used for both separated and disperse phases and which is shown to degenerate into a standard NDF in the disperse region. In the last section, we finally propose a numerical procedure based on some existing computer graphics algorithms to compute the curvatures [41, 42], as well as a new numerical approach to spatially average these quantities and then compute the various statistical distributions (SDF or NDF, based on a characteristic spatial averaging size) from the values of a Level Set function. These new algorithms are eventually applied to the post-processing of some DNS simulations, obtained with the ARCHER code, developed at CORIA laboratory [4]. The meaning of the obtained numerical results is two fold: they assess the theoretical part of this work by proving that we can indeed turn an interfacial information into a statistics of countable objects, but they also pave the way to a new way of analyzing DNS of interfacial flows.

2. Surface element properties and probabilistic description of the gas-liquid interface

Immiscible two-phase flows, such as gas-liquid mixtures, are characterized by the presence of a sharp interface. Indeed, the gas-liquid interface thickness being of the order of the molecular mean free path ($\lambda = 10$ nm), it is smaller than the microscopic length scales of the vast majority of two-phase flow applications. Thus, at macroscopic scale, this interface can be represented as a 2D dynamic surface embedded in a 3D domain. In the following, we consider a two-phase flow (gas and liquid) within a finite 3D domain Ω_x. Let us denote by $\mathbf{S}_I(t)$ the moving surface that separates both phases. First, we do not make any assumption on the flow topology (separated or disperse). We start by defining a 2D surface and some intrinsic geometrical variables in subsections 2.1-2.3. Then in subsection 2.4, we introduce a statistical description of the gas-liquid interface similar to Pope's description of flames dynamics and propagation [39].

2.1. Surface definition

Since we are dealing with disperse and separated phases in the same domain, the moving surface $\mathbf{S}_I(t)$ is not necessarily a connected set: in general it consists in a set of closed (disperse phase) and unclosed (bulk phase) connected sub-surfaces. Therefore, the global surface $\mathbf{S}_I(t)$ can be written as a union of connected sub-surfaces $\mathbf{S}_i(t)$:

$$\mathbf{S}_I(t) = \bigcup_{i=1}^{N_{\max}} \mathbf{S}_i(t), \tag{1}$$

that are separated in the sense that, for $i \neq j$:

$$\min_{(\boldsymbol{x},\boldsymbol{y})\in\mathbf{S}_i(t)\times\mathbf{S}_j(t)} (\|\boldsymbol{x}-\boldsymbol{y}\|) > 0.$$

The surface can be defined as the set of zeros of a time-space function $(t;\boldsymbol{x}) \mapsto g(t;\boldsymbol{x})$:

$$\mathbf{S}_I(t) = \{\boldsymbol{x} \in \Omega_x; \quad g(t;\boldsymbol{x}) = 0\}. \tag{2}$$

The function g satisfies the following kinematic equation:

$$\frac{\partial g}{\partial t} + \boldsymbol{V}_I^g \cdot \boldsymbol{\nabla}(g) = 0, \tag{3}$$

where $\boldsymbol{V}_I^g(t;\boldsymbol{x})$ is an interface velocity, whose definition is discussed thereafter.

From now on, we suppose that each sub-surface $\mathbf{S}_i$ is a C^2 oriented surface, meaning that the space function $g(t;.)$ is a C^2 differentiable function. The orientation is chosen such that the gradient $\boldsymbol{\nabla} g(t;\boldsymbol{x})$ at the interface points ($g(t;\boldsymbol{x}) = 0$) is strictly oriented toward the gaseous phase.

2.2. Intrinsic gas-liquid interface variables

The aim of this paragraph is to introduce some local intrinsic properties of the interface, independant of the surface definition: the choice of the parametrization function g, among others. These quantities will be useful for setting a statistical description of the interface.

2.2.1. Normal vector and tangent plane

Let us consider a point on the surface $\boldsymbol{x}_i \in \mathbf{S}_I(t)$. Using (2), the normal vector at $\boldsymbol{x}_i$ is given by:

$$\boldsymbol{N}(t,\boldsymbol{x}_i) = \frac{\boldsymbol{\nabla}_{\boldsymbol{x}} g(t;\boldsymbol{x}_i)}{\|\boldsymbol{\nabla}_{\boldsymbol{x}} g(t;\boldsymbol{x}_i)\|}. \tag{4}$$

The tangent plane to the surface at $\boldsymbol{x}_i$ is the unique plan orthogonal to $\boldsymbol{N}$ and passing by $\boldsymbol{x}_i$.

2.2.2. Curvatures

Curvatures are defined as the infinitesimal variations of $(t,\boldsymbol{x}) \mapsto \boldsymbol{N}(t,\boldsymbol{x})$ when $\boldsymbol{x}$ follows a path over the interface. These variations can be expressed as a function of the Hessian matrix $\mathcal{H}(g)$ of the function $g(t;.)$,see [43] for more details:

$$\boldsymbol{\nabla}_{\boldsymbol{x}} \boldsymbol{N}^T = -\frac{1}{\|\boldsymbol{\nabla}_{\boldsymbol{x}} g\|}(\mathbf{I}_3 - \boldsymbol{N} \otimes \boldsymbol{N}^T)\mathcal{H}(g), \tag{5}$$

where $\mathcal{H}(g)$ is given by:

$$\mathcal{H}(g)(t;\boldsymbol{x}) = \boldsymbol{\nabla}_{\boldsymbol{x}}(\boldsymbol{\nabla}_{\boldsymbol{x}} g) = \left(\frac{\partial^2 g}{\partial x_j \partial x_k}(t;\boldsymbol{x})\right)_{j,k=1\ldots3}, \tag{6}$$

and $\mathbf{I}_3$ is the identity matrix.

It can be shown that there exists an orthonormal basis $\{\boldsymbol{e}_1^*, \boldsymbol{e}_2^*\}$ of the tangent plane at the surface point $\boldsymbol{x}_i$, such that the restriction of the matrix $\boldsymbol{\nabla}_{\boldsymbol{x}} \boldsymbol{N}^T$ to the tangent plane is a 2×2 diagonal matrix [43]. In other words, in the orthonormal basis $\{\boldsymbol{e}_1^*, \boldsymbol{e}_2^*, \boldsymbol{N}\}$, $\boldsymbol{\nabla}_{\boldsymbol{x}} \boldsymbol{N}^T$ reads:

$$\boldsymbol{\nabla}_{\boldsymbol{x}} \boldsymbol{N}^T = \begin{pmatrix} \kappa_1 & 0 & \sigma_1 \\ 0 & \kappa_2 & \sigma_2 \\ 0 & 0 & 0 \end{pmatrix}, \tag{7}$$

where $\kappa_1 \geq \kappa_2$ are the two principal curvatures and (σ_1, σ_2) are two real variables. The eigenvectors $\{\boldsymbol{e}_1^*, \boldsymbol{e}_2^*\}$ corresponding to the eigenvalues (κ_1, κ_2) are called the *principal directions* of the surface at $\boldsymbol{x}_i$.

Instead of using the two principal curvatures, one can consider the *mean curvature* H and the *Gauss curvature* G, defined by:

$$\begin{array}{rcl} H & = & \dfrac{1}{2}(\kappa_1 + \kappa_2), \\ G & = & \kappa_1 \kappa_2. \end{array} \tag{8}$$

Indeed, the mapping

$$\left\{ \begin{array}{ccc} \left\{(\kappa_1, \kappa_2) \in \mathbb{R}^2;\ \kappa_1 \geq \kappa_2\right\} & \longrightarrow & \left\{(H, G) \in \mathbb{R}_+^2;\ H^2 \geq G\right\} \\ (\kappa_1, \kappa_2) & \longmapsto & (H, G) \end{array} \right. , \tag{9}$$

is one-to-one.

2.2.3. Area density measure

The last quantity needed in the following is an evaluation of the interface area within any control volume. For this purpose, we introduce the *area density measure* as follows, see [44] and related works:

$$\delta_I(t; \boldsymbol{x}) = \|\boldsymbol{\nabla}_{\boldsymbol{x}} g\|\, \delta(g(t, \boldsymbol{x})), \tag{10}$$

where δ denotes the Dirac measure. Consequently, for any volume $\mathcal{V}$, the area $A_{\mathcal{V}}(t)$ of surface contained in $\mathcal{V}$ at time t is given by:

$$A_{\mathcal{V}}(t) = \int_{\Omega_x} \mathbb{1}_{\mathcal{V}}(\boldsymbol{x}) \delta_I(t; \boldsymbol{x}),$$

where $\mathbb{1}_{\mathcal{V}}(\boldsymbol{x})$ is the characteristic function of the volume $\mathcal{V}$. It is important to note that the measure δ_I does not depend on the choice of g. It is an intrinsic property of the interface.

2.2.4. Interface velocity

The interface velocity is not uniquely defined. It may depend on the definition of the interface, and in particular on the choice of the parametrization function g. However, as underlined in [38], the evolution of the interface with equation (3) only depends on the normal component of $\boldsymbol{V}_I^g$. Then, we introduce $V_I = \boldsymbol{V}_I^g \cdot \boldsymbol{N}$, that is unambiguously defined, and the interface velocity reads:

$$\boldsymbol{V}_I = V_I \boldsymbol{N}. \tag{11}$$

In the case when the interface lies in a medium of velocity-field $\mathbf{U}(t, \boldsymbol{x})$, and propagate within this medium, at a velocity $V_e \boldsymbol{N}$, the interface velocity reads [39]:

$$V_I = (\mathbf{U} \cdot \boldsymbol{N}) + V_e.$$

Think of a flame that separates burnt and unburnt gases. The flame speed V_e depends on the chemical reactions rates. In the case of two-phase flows, V_e may characterize the rate of phase transitions, such as evaporation or condensation.

2.3. Time evolution of the interfacial variables

In this paragraph, we present the evolution equations for surface element properties based on the works of Drew [38]. Let us mention that the choice in the definition of the interface velocity affects the expression of the evolution laws for the curvatures and the area density measure. Here we consider the interface velocity defined by (11). Then, the time evolution of the curvatures can be expressed as follows:

$$\begin{aligned} \dot{H} &= -\frac{1}{2}\nabla_T^2(V_I) - (2H^2 - G)V_I, \\ \dot{G} &= -H\nabla_T^2(V_I) + \sqrt{H^2 - G}\left(\frac{\partial^2 V_I}{\partial y_1^{*2}} - \frac{\partial^2 V_I}{\partial y_2^{*2}}\right) - 2\,H\,G\,V_I, \end{aligned} \tag{12}$$

where $\dot{\bullet} = \partial_t \bullet + \boldsymbol{V}_I \cdot \nabla_{\boldsymbol{x}} \bullet$, denotes the Lagrangian time derivative, $\nabla_T^2 = \partial_{y_1}^2 + \partial_{y_2}^2$ is the tangential Laplacian operator (y_1 and y_2 can be any two orthonormal directions tangential to the surface), and y_k^* is the coordinate along the principal directions $\boldsymbol{e}_k^*$, $k = 1, 2$. In AppendixA, we derive the equation for δ_I. This equation reads:

$$\dot{\delta}_I = -\left(\nabla_{\boldsymbol{x}} \cdot \boldsymbol{V}_I\right)\delta_I + 2H\,V_I\,\delta_I. \tag{13}$$

In equation (13), one can identify the second term in the right-hand side with the *stretching rate* $\dot{\mathcal{S}}$, which is defined in Pope [39] as an intrinsic property. For an interface velocity that is normal to the interface, its equation reads:

$$\dot{\mathcal{S}} = 2H\,V_I. \tag{14}$$

The system (12) remains unclosed, because of the second order derivatives of the interfacial velocity in the two principal directions. For future works, these terms need to be modeled, but this is not the objective of the present work. An interpretation of the different terms occurring in the system of equation (12) can be found in [38].

2.4. General statistical description of the interface

Now, we propose to introduce a general statistical description of a gas-liquid interface, that is useful when the exact location of the interface is not known, like in turbulent flows [39] or in two-phase transition zones. Obviously, the statistical description of the interface can not be restricted to one geometrical variable, as is often done for disperse phases. Indeed, when assuming that droplets are spherical, the information about the droplets radii is enough to describe the interface geometry. This is however not the case with a general interface, such as one described by (1). In the following, we propose to use the mean and Gauss curvatures, as well as the interface velocity, to characterize the local interface properties and their evolution. These variables will be called the phase-space variables:

$$\widehat{\boldsymbol{\xi}} = (\widehat{H}, \widehat{G}, \widehat{\boldsymbol{V}_I}),$$

and $\Omega_{\boldsymbol{\xi}}$ is the set of values that can be attained by any realization $\widehat{\boldsymbol{\xi}} = \boldsymbol{\xi}(t, \boldsymbol{x})$ at time t and position $\boldsymbol{x}$. Moreover we need to define an appropriate probabilistic measure. In the case of a general gas-liquid interface, we adopt a measure based on the area

concentration of the geometric properties of the interface. Let us consider the surface density function (SDF) $F(t,\boldsymbol{x};\widehat{\boldsymbol{\xi}})$ [39], defined as follows: the quantity $F(t,\boldsymbol{x};\widehat{\boldsymbol{\xi}})d^5\widehat{\boldsymbol{\xi}}d^3\boldsymbol{x}$ measures the probable surface area present in the spatial volume $d^3\boldsymbol{x}$ around $\boldsymbol{x}$ and in the phase-space volume $d^5\widehat{\boldsymbol{\xi}}$ around $\widehat{\boldsymbol{\xi}}$. The notion "probable" is used here in the sense of an ensemble averaging over different realizations, as defined by Drew [31]. To clarify this concept of SDF, let us first give a definition of the SDF for one realization, namely the *fine-grain* SDF, F':

$$F'(t,\boldsymbol{x};\widehat{\boldsymbol{\xi}}) = \delta_I(t,\boldsymbol{x})\delta(\widehat{\boldsymbol{\xi}} - \boldsymbol{\xi}(t,\boldsymbol{x})). \tag{15}$$

Secondly, the SDF is defined as an ensemble average over all the realizations:

$$F(t,\boldsymbol{x};\widehat{\boldsymbol{\xi}}) =< F'(t,\boldsymbol{x};\widehat{\boldsymbol{\xi}}) >, \tag{16}$$

where $< \bullet >$ is the ensemble average operator.

Using the same procedure as in [39], we can derive the following transport equation with a source term:

$$\partial_t F + \nabla_{\boldsymbol{x}} \cdot \{\widehat{\boldsymbol{V}_I} F\} + \nabla_{\widehat{\boldsymbol{\xi}}} \cdot \{< \dot{\boldsymbol{\xi}} >_c F\} =< \dot{\mathcal{S}} >_c F, \tag{17}$$

where the *conditional expectation* of a scalar ψ is defined by:

$$< \psi >_c = \frac{< \psi F'(t,\boldsymbol{x};\widehat{\boldsymbol{\xi}}) >}{F(t,\boldsymbol{x};\widehat{\boldsymbol{\xi}})}.$$

The SDF evolves due to two main contributions: the left-hand side of equation (17) contributes to the evolution of F in the phase-space Ω_ξ and in the physical space Ω_x. This evolution is expressed as divergences of conservative fluxes. The source terms of the right-hand side of equation (17) express the evolution of the surface area due to stretching.

The conditional expectations of $\dot{H}$, $\dot{G}$ and $\dot{\mathcal{S}}$ may be obtained from their Lagrangian time evolution (12) by applying the ensemble averaging and by using the linearity of the average operator, as well as Gauss and Leibniz rules:

$$< \lambda a + b >= \lambda < a > + < b >, \quad < \partial_t a >= \partial_t < a > \quad \text{and} \quad < \partial_x a >= \partial_x < a > .$$

Then, the averaged evolution equations read:

$$\begin{aligned}
< \dot{H} >_c &= -\frac{1}{2} < \nabla_T^2(V_I) >_c - (2\widehat{H}^2 - \widehat{G})\,(\widehat{\boldsymbol{V}_I} \cdot < \boldsymbol{N} >_c), \\
< \dot{G} >_c &= -\widehat{H} < \nabla_T^2(V_I) >_c + \sqrt{\widehat{H}^2 - \widehat{G}} \left\langle \frac{\partial^2 V_I}{\partial y_1^{*2}} - \frac{\partial^2 V_I}{\partial y_2^{*2}} \right\rangle_c - 2\widehat{H}\widehat{G}\,(\widehat{\boldsymbol{V}_I} \cdot < \boldsymbol{N} >_c), \\
< \dot{\mathcal{S}} >_c &= 2\widehat{H}\,(\widehat{\boldsymbol{V}_I} \cdot < \boldsymbol{N} >_c).
\end{aligned} \tag{18}$$

One can note that some terms are unclosed in these equations. These are the conditional expectations of:

- the normal vector $< \boldsymbol{N} >_c$,

- the second order derivatives of the interfacial velocity $< \nabla_T^2(V_I) >_c$,
- the evolution of the interfacial velocity $< \dot{\boldsymbol{V}}_I >_c$.

These terms need to be modeled and related to the internal flow dynamics of the gas and liquid phases.

2.5. Averaged quantities and moments of the SDF

The numerical resolution of equation (17) is unreachable for most applications because of the large dimension of the phase space $\Omega_{\boldsymbol{\xi}}$. In fact, solving the exact SDF would provide a level of detail on the flow, which is often not needed: the large amount of produced data may hide the prevailing macroscopic features we are looking for. Therefore, we only aim at predicting some macroscopic variables of the flow, that ensure a satisfactory result for most industrial applications. Drew [38] derived Eulerian equations for the evolution of the following averaged quantities: the expected surface density $\Sigma(t, \boldsymbol{x})$ and the interfacial-expected mean and Gauss curvatures, $\widetilde{H}$, $\widetilde{G}$.

In terms of moments of the SDF, $\Sigma(t, \boldsymbol{x})$, $\widetilde{H}$ and $\widetilde{G}$ can be expressed as follows:

$$\begin{array}{rcl} \Sigma(t,\boldsymbol{x}) & = & M_{0,0,\boldsymbol{0}}(t,\boldsymbol{x}), \\ \Sigma(t,\boldsymbol{x})\widetilde{H} & = & M_{1,0,\boldsymbol{0}}(t,\boldsymbol{x}), \\ \Sigma(t,\boldsymbol{x})\widetilde{G} & = & M_{0,1,\boldsymbol{0}}(t,\boldsymbol{x}), \end{array} \tag{19}$$

where the moments read:

$$M_{i,j,\boldsymbol{l}}(t,\boldsymbol{x}) = \int_{\Omega_{\boldsymbol{\xi}}} H^i G^j V_{I,x}^{l_x} V_{I,y}^{l_y} V_{I,z}^{l_z} F(t,\boldsymbol{x};\widehat{\boldsymbol{\xi}}) d^5\widehat{\boldsymbol{\xi}}, \tag{20}$$

and $\boldsymbol{l} = (l_x, l_y, l_z)$.

Then, by considering the successive moments of the SDF equation (17), we can derive the evolution equations for these three quantities of interest:

$$\begin{array}{rcl} \partial_t\Sigma + \boldsymbol{\nabla}_{\boldsymbol{x}} \cdot \left\{\Sigma\, \overline{\boldsymbol{V}_I}\right\} & = & \int_{\widehat{\boldsymbol{\xi}}} < \dot{\mathcal{S}} >_c F(t,\boldsymbol{x};\widehat{\boldsymbol{\xi}})\, d^5\widehat{\boldsymbol{\xi}}, \\ \partial_t\Sigma\widetilde{H} + \boldsymbol{\nabla}_{\boldsymbol{x}} \cdot \left\{\Sigma\, \widetilde{H}\, \overline{\boldsymbol{V}_I}\right\} & = & \boldsymbol{\nabla}_{\boldsymbol{x}} \cdot \left\{\Sigma\widetilde{H}(\overline{\boldsymbol{V}_I} - \overline{\boldsymbol{V}_I}^H)\right\} + \int_{\widehat{\boldsymbol{\xi}}} < \dot{\mathcal{S}} + \dot{H}/\widehat{H} >_c \widehat{H} F(t,\boldsymbol{x};\widehat{\boldsymbol{\xi}})\, d^5\widehat{\boldsymbol{\xi}}, \\ \partial_t\Sigma\widetilde{G} + \boldsymbol{\nabla}_{\boldsymbol{x}} \cdot \left\{\Sigma\, \widetilde{G}\, \overline{\boldsymbol{V}_I}\right\} & = & \boldsymbol{\nabla}_{\boldsymbol{x}} \cdot \left\{\Sigma\widetilde{G}(\overline{\boldsymbol{V}_I} - \overline{\boldsymbol{V}_I}^G)\right\} + \int_{\widehat{\boldsymbol{\xi}}} < \dot{\mathcal{S}} + \dot{G}/\widehat{G} >_c \widehat{G} F(t,\boldsymbol{x};\widehat{\boldsymbol{\xi}})\, d^5\widehat{\boldsymbol{\xi}}. \end{array} \tag{21}$$

We can notice three types of averaged interfacial velocity that read:

$$\begin{array}{rcl} \Sigma\, \widetilde{\boldsymbol{V}_I} & = & \int_{\widehat{\boldsymbol{\xi}}} \widehat{\boldsymbol{V}_I} F(t,\boldsymbol{x};\widehat{\boldsymbol{\xi}})\, d^5\widehat{\boldsymbol{\xi}}, \\ \Sigma\, \widetilde{H}\, \overline{\boldsymbol{V}_I}^H & = & \int_{\widehat{\boldsymbol{\xi}}} \widehat{\boldsymbol{V}_I}\widehat{H} F(t,\boldsymbol{x};\widehat{\boldsymbol{\xi}})\, d^5\widehat{\boldsymbol{\xi}}, \\ \Sigma\, \widetilde{G}\, \overline{\boldsymbol{V}_I}^G & = & \int_{\widehat{\boldsymbol{\xi}}} \widehat{\boldsymbol{V}_I}\widehat{G} F(t,\boldsymbol{x};\widehat{\boldsymbol{\xi}})\, d^5\widehat{\boldsymbol{\xi}}. \end{array} \tag{22}$$

Using the time evolution of both curvatures and of the stretch factor (12) in the system of equations (21), we can show that this system is equivalent to the system

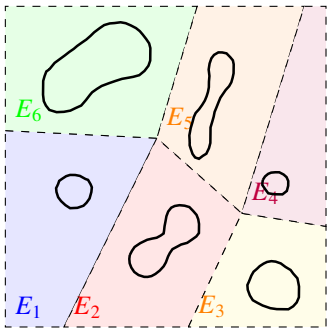

Figure 1: Illustration of the spatial decomposition, with subspaces containing only one particle.

derived by Drew in [38]. However, two closure issues need to be tackled at two different stages for future works. First, we need time evolution laws to close the conditional averages ($< \dot{H} >_c, < \dot{G} >_c, < \dot{\mathcal{S}} >_c$), as already mentioned for the transport equation of the SDF. Next, we need to propose a procedure to reconstruct the SDF from the known moments.

3. Statistical description of the gas-liquid interface for a disperse phase

3.1. Surface density function in the context of discrete particles

The SDF measures the pointwise probable area concentration for a probabilistic event, which is characterized by the phase space variables $\widehat{\boldsymbol{\xi}} = \{\widehat{H}, \widehat{G}, \widehat{\boldsymbol{V}_I}\} \in \Omega_{\boldsymbol{\xi}}$ and is evaluated at a local point $\boldsymbol{x} \in \Omega_x$. This probabilistic description is a pointwise description of the interface, which makes it general and valid for both separated and disperse phases. However, in the case of a disperse flow, a point-particle approach is usually considered. Each particle, droplet or bubble, is reduced to a point, characterized by some averaged and global quantities, such as: the velocity of the center of mass or the particle size (measured by volume, surface area or diameter), or any other quantity of interest. The statistics are conducted on a number of objects. In order to adapt the statistical approach presented in the previous section to a discrete formalism for a disperse phase, we first define interfacial quantities that are averaged over the surface of each particle. Then, we define a *discrete surface density function* that may characterize the dispersion in size and in shape of the population of particles.

Let us consider an isolated particle p_k of surface $\mathbb{S}_k$, supposed to be smooth. Let us also consider a partition of the domain $\Omega_x = \bigcup_{k=1}^{N_{max}} E_k$, such that each sub-domain E_k contains exactly one particle p_k, as illustrated in Figure 1. For a quantity $\phi(t, \boldsymbol{x})$, that can be a scalar (like curvatures) or a vector (like a velocity), we define its interface average $\overline{\phi}_k(t, \boldsymbol{x})$ over the particle surface $\mathbb{S}_k$ as follows:

$$\overline{\phi}_k(t, \boldsymbol{x}_k) = \frac{1}{S_k} \int_{\boldsymbol{x} \in E_k} \phi(t, \boldsymbol{x}) \delta_I(t, \boldsymbol{x}) d^3\boldsymbol{x}, \tag{23}$$

where S_k is the total surface area of the particle:

$$S_k = \int_{\boldsymbol{x}\in E_k} \delta_I(t,\boldsymbol{x}) d^3\boldsymbol{x},$$

and $\boldsymbol{x}_k$ its center of mass.

From now on, we consider each particle p_k as punctual, located at its center of mass $\boldsymbol{x}_k(t)$, having a surface area S_k and the averaged interface properties $\overline{\boldsymbol{\xi}}_k = \{\overline{H}_k, \overline{G}_k, \overline{V}_{Ik}\}$. We define the discrete SDF by:

$$F^d(t,\boldsymbol{x},\widehat{\boldsymbol{\xi}}) =< \sum_{k=1}^{N_{max}} S_k(t)\delta(\boldsymbol{x}-\boldsymbol{x}_k(t))\delta(\widehat{\boldsymbol{\xi}}-\overline{\boldsymbol{\xi}}_k(t)) > \tag{24}$$

where N_{max} is the maximum number of particles in the domain Ω_x over all realizations. One can note that the average interface velocity is the velocity of the surface barycenter point defined by $\widetilde{\boldsymbol{x}}_k = 1/S_k \int_{S_k} \boldsymbol{x} dS(\boldsymbol{x})$ and it is different in general case of the center of mass $\boldsymbol{x}_k$. The defined average interface velocity can be written as follows:

$$\overline{\boldsymbol{V}_{Ik}}(t) = \frac{d\boldsymbol{x}_k(t)}{dt} + V_k^{''}(t),$$

where $V_k^{''}(t)$ is a fluctuation velocity, that stands for the particle shape deformations. Since we have chosen to locate the particles at their centers of mass, which is more practical as far as the particle dynamics is considered, we propose a different definition of the average interface velocity where we simply track the droplets by the velocity of their center of mass, neglect the fluctuation velocity (which can be considered as small in this coarse-graining process), and we write:

$$\overline{\boldsymbol{V}_{Ik}}(t) = \frac{d\boldsymbol{x}_k(t)}{dt}. \tag{25}$$

The discrete SDF (24) verifies a similar transport equation as (17):

$$\partial_t F^d + \nabla_{\boldsymbol{x}} \cdot \{\widehat{\boldsymbol{V}_I} F^d\} + \boldsymbol{\nabla}_{\widehat{\boldsymbol{\xi}}} \cdot \{< \dot{\overline{\boldsymbol{\xi}}} >_c F^d\} =< \dot{\overline{\mathcal{S}}} >_c F^d. \tag{26}$$

where $\dot{\overline{\mathcal{S}}} = \dot{S}_k(t)/S_k(t)$ if $\boldsymbol{x} = \boldsymbol{x}_k$ and $\dot{\overline{\mathcal{S}}} = 0$ otherwise. Once more, the time evolution of the averaged curvatures needs to be modeled in order to close the system of equations. This is work in progress and is out of the scope of the present paper.

The "localized" SDF defined in section 2.4 and the discrete SDF are two different functions. Nonetheless, they contain similar pieces of information about the gas-liquid interface properties. Indeed, both functions provide the probable surface area of the interface having some geometrical properties given by the phase-space variables. For the "localized" SDF, the phase-space variables are given by the localized interface properties at a surface point, while for the discrete SDF, we have considered interface properties averaged by object (particle). The link between the two functions can be seen through the first order moments of the two functions:

Proposition 3.1. *Given a subdomain $E \subset \Omega_x$, such that its border does not cut any particle, the integral over this subdomain of the zeroth and first order moments of the two functions satisfy:*

$$\begin{aligned} \int_{\boldsymbol{x}\in E}\int_{\widehat{\boldsymbol{\xi}}\in\Omega_{\xi}} F(t,\boldsymbol{x};\widehat{\boldsymbol{\xi}})\,d^5\widehat{\boldsymbol{\xi}}d^3\boldsymbol{x} &= \int_{\boldsymbol{x}\in E}\int_{\widehat{\boldsymbol{\xi}}\in\Omega_{\xi}} F^d(t,\boldsymbol{x};\widehat{\boldsymbol{\xi}})\,d^5\widehat{\boldsymbol{\xi}}d^3\boldsymbol{x} \\ \int_{\boldsymbol{x}\in E}\int_{\widehat{\boldsymbol{\xi}}\in\Omega_{\xi}} \widehat{\boldsymbol{\xi}}_l F(t,\boldsymbol{x};\widehat{\boldsymbol{\xi}})\,d^5\widehat{\boldsymbol{\xi}}d^3\boldsymbol{x} &= \int_{\boldsymbol{x}\in E}\int_{\widehat{\boldsymbol{\xi}}\in\Omega_{\xi}} \widehat{\boldsymbol{\xi}}_l F^d(t,\boldsymbol{x};\widehat{\boldsymbol{\xi}})\,d^5\widehat{\boldsymbol{\xi}}d^3\boldsymbol{x} \end{aligned} \tag{27}$$

where $\widehat{\boldsymbol{\xi}}_l \in \left\{\widehat{H},\widehat{G},\widehat{V}_{Ix},\widehat{V}_{Iy},\widehat{V}_{Iz}\right\}$.

Proof:. We illustrate this result for a moment of order one on G and zero on the other phase variables ($\widehat{\boldsymbol{\xi}}_l = \widehat{G}$):

$$\begin{aligned} \int_{\boldsymbol{x}\in E}\int_{\widehat{\boldsymbol{\xi}}\in\Omega_{\xi}} \widehat{G}F(t,\boldsymbol{x};\widehat{\boldsymbol{\xi}})\,d^5\widehat{\boldsymbol{\xi}}d^3\boldsymbol{x} &= \int_{\boldsymbol{x}\in E}\int_{\widehat{\boldsymbol{\xi}}\in\Omega_{\xi}} \widehat{G} < \delta_I(\boldsymbol{x})\delta(\widehat{\boldsymbol{\xi}} - \boldsymbol{\xi}(t,\boldsymbol{x})) > \, d^5\widehat{\boldsymbol{\xi}}d^3\boldsymbol{x} \\ &= < \int_{\boldsymbol{x}\in E} G(t;\boldsymbol{x})\,\delta_I(\boldsymbol{x})\,d^3\boldsymbol{x} > \\ &= < \sum_k \int\limits_{\boldsymbol{x}\in E_k\cap E} G(t;\boldsymbol{x})\,\delta_I(\boldsymbol{x})\,d^3\boldsymbol{x} > \\ &= < \sum_{\{k;\,\boldsymbol{x}_k(t)\in E\}} S_k\overline{G}_k > \\ &= < \sum_{\{k;\,\boldsymbol{x}_k(t)\in E\}} S_k \int_{\boldsymbol{x}\in E_k}\int_{\widehat{\boldsymbol{\xi}}\in\Omega_{\xi}} \widehat{G}\delta(\widehat{\boldsymbol{\xi}} - \overline{\boldsymbol{\xi}}_k)\delta(\boldsymbol{x} - \boldsymbol{x}_k(t))d^5\widehat{\boldsymbol{\xi}}\,d^3\boldsymbol{x} > \\ &= \int_{\boldsymbol{x}\in E}\int_{\widehat{\boldsymbol{\xi}}\in\Omega_{\xi}} \widehat{G}F^d(t,\boldsymbol{x},\widehat{\boldsymbol{\xi}})\,d^5\widehat{\boldsymbol{\xi}}d^3\boldsymbol{x}. \end{aligned} \tag{28}$$

□

We recall that the zeroth and first-order moments are related to the expected surface density and the two curvatures $(\Sigma, \Sigma\widetilde{H}, \Sigma\widetilde{G})$, defined in (19), and to the expected interface velocity, defined in the first equation of (22). In this work, we give a great importance to these quantities because they contain some topological information about the gas-liquid interface, such as the number density of particles, as we will show in next section. From now on, we call these quantities the "*topological moments*" and we underline that any future definition of a new SDF should preserve these moments.

3.2. Link between the discrete SDF and a NDF: derivation of a Williams-Boltzmann-like equation

Let us now present the relation between the discrete SDF (24) and a number density function (NDF) for particles, using a geometrical property of the averaged Gauss curvature, known as the *Gauss-Bonnet formula*.

Let M be a 3D bounded object and $\mathbb{S}(M)$ its surrounding closed surface, supposed to be smooth. The Gauss-Bonnet formula applied to $\mathbb{S}(M)$ states that [45]:

$$\int_{\boldsymbol{x}\in\mathbb{S}(M)} G(\boldsymbol{x})dS(\boldsymbol{x}) = 2\pi\chi(M), \tag{29}$$

where $\chi(M)$ is the Euler characteristic of M and is a topological invariant, meaning that two homeomorphic objects[1] have the same Euler characteristic. In the following, we consider smooth particle surfaces, that are all homeomorphic to a sphere, whose Euler characteristic is 2. Therefore, we can relate the averaged Gauss curvature over the surface of a particle p_k to its surface area by:

$$S_k = \frac{4\pi}{\overline{G}_k}. \tag{30}$$

Since $\frac{S_k \overline{G}_k}{4\pi} = 1$ for each particle, we are able to count the total number of particles, just by looking at the interface average of G. Then, we can derive a relation between the discrete SDF F^d and a Number Density Function (NDF) f. This relation is given by the following proposition.

Proposition 3.2. *When the two-phase flow is purely disperse, the distribution function* $\frac{\widehat{G}}{4\pi} F^d(t, \boldsymbol{x}; \widehat{\boldsymbol{\xi}})$ *is equal to the NDF* $f(t, \boldsymbol{x}; \widehat{\boldsymbol{\xi}})$ *for a phase space made of the averaged curvatures and interface velocity* $\widehat{\boldsymbol{\xi}} = \{\widehat{H}, \widehat{G}, \widehat{V_I}\}$*:*

$$\frac{\widehat{G}}{4\pi} F^d(t, \boldsymbol{x}; \widehat{\boldsymbol{\xi}}) = f(t, \boldsymbol{x}; \widehat{\boldsymbol{\xi}}) \tag{31}$$

Proof:.

$$\begin{aligned}
\frac{\widehat{G}}{4\pi} F^d(t, \boldsymbol{x}; \widehat{\boldsymbol{\xi}}) &= < \sum_{k=1}^{N_{max}} S_k(t) \delta(\boldsymbol{x} - \boldsymbol{x}_k(t)) \left\{ \frac{\widehat{G}}{4\pi} \right\} \delta(\widehat{\boldsymbol{\xi}} - \overline{\boldsymbol{\xi}}_k(t))) >, \\
&= < \sum_{k=1}^{N_{max}} S_k(t) \delta(\boldsymbol{x} - \boldsymbol{x}_k(t)) \left\{ \frac{\overline{G}_k(t)}{4\pi} \right\} \delta(\widehat{\boldsymbol{\xi}} - \overline{\boldsymbol{\xi}}_k(t)) >, \\
&= < \sum_{k=1}^{N_{max}} \delta(\boldsymbol{x} - \boldsymbol{x}_k(t)) \delta(\widehat{\boldsymbol{\xi}} - \overline{\boldsymbol{\xi}}_k(t)) >, \\
&= f(t, \boldsymbol{x}; \widehat{\boldsymbol{\xi}}).
\end{aligned} \tag{32}$$

The second line is obtained by using the equality: $u_i \delta(\boldsymbol{u} - \boldsymbol{v}) = v_i \delta(\boldsymbol{u} - \boldsymbol{v})$ for all $\boldsymbol{u}, \boldsymbol{v} \in \mathbb{R}^m$ and $1 \leq i \leq m$ where m is the space dimension. □

From the transport equation of the discrete SDF (26), we can derive a General Population Balance Equation (GPBE) for $f(t, \boldsymbol{x}; \widehat{\boldsymbol{\xi}})$, that is similar to the Williams-Boltzmann equation:

$$\partial_t f + \nabla_{\boldsymbol{x}} \cdot \{\widehat{V_I} f\} + \nabla_{\widehat{\boldsymbol{\xi}}} \cdot \{< \dot{\widehat{\boldsymbol{\xi}}} >_c f\} = \left(< \dot{\overline{\mathcal{S}}} >_c + < \frac{\dot{\overline{G}}}{\overline{G}} >_c \right) f. \tag{33}$$

[1] In the mathematical field of topology, a homeomorphism also called a homeomorphic transformation is a continuous function between topological spaces that has a continuous inverse function.

The right-hand term of equation 33 behaves as a source term. We can relate this term to topological evolutions of the Euler characteristic of droplets due to fragmentation, coalescence, etc.

Let us now consider a set of droplets that do not break up, nor coalesce and which are all the time homeomorphic to spheres. Using the Gauss-Bonnet result (30), we can show that:

$$\dot{\overline{\mathcal{S}}} = -\frac{\dot{\overline{G}}(t)}{\overline{G}(t)}. \tag{34}$$

Therefore, without break-up nor coalescence, equation (33) reduces to:

$$\partial_t f + \nabla_{\boldsymbol{x}} \cdot \{\widehat{\boldsymbol{V}_I} f\} + \nabla_{\widehat{\boldsymbol{\xi}}} \cdot \{< \dot{\widehat{\boldsymbol{\xi}}} >_c f\} = 0. \tag{35}$$

Equation (35) represents the time evolution of the particles NDF due to transport in physical space at the velocity of their center of mass, and the evolution of the internal variables, which represent the particle surface deformations and their acceleration by interaction with the carrier gas.

From equation (35), one can derive the system of equations that describes the evolution of the first moments of the NDF f similar to the one derived in 21. In the appendix AppendixB, we propose a simplified closed model of such system in the case of a polydisperse evaporating spray, where the droplets are supposed to remain spherical at any time.

From now on, we omit the subscript $\widehat{\bullet}$ for the phase-space variables.

4. From separated to disperse phases: a generalized statistical approach through spatial averaging.

In section 3.1, we have drawn a link between the NDF and the discrete SDF in the context of a discrete formalism. However, the discrete SDF supposes that we are able to isolate the droplets/ligaments in a certain manner. Therefore, it is not yet obvious that a statistical description of the gas-liquid interface may describe a spray evolving under Williams-Boltzmann's equation. In this section, we show how a new SDF, that is spatially averaged, degenerates to the discrete SDF (24), when the liquid phase is dispersed and dilute. We take advantage of this new relation to design a numerical approach for the analysis of DNS computations of gas-liquid interfaces. This numerical tool is thus used to automatically and efficiently compute statistics of populations of deformed objects.

4.1. Averaged interfacial quantities and appropriate phase space variables

The objective of this paragraph is to develop a specific spatial averaging procedure, that satisfies some properties. First, the spatial averaging is applied separately for each realization on the phase variables $\boldsymbol{\xi}(t, \boldsymbol{x})$. Thus, we define the Averaged SDF (ASDF) as follows:

$$\mathrm{F}^a(t, \boldsymbol{x}; \boldsymbol{\xi}) =< \delta_I(t, \boldsymbol{x})\, \delta(\boldsymbol{\xi} - \widetilde{\boldsymbol{\xi}}(t, \boldsymbol{x})) > . \tag{36}$$

Second the averaged space variables $\widetilde{\boldsymbol{\xi}}(t, \boldsymbol{x})$ are defined so as to satisfy the following properties:

A. the ASDF preserves the space integral of the classical SDF first order moments as in Proposition 3.1. This property reads:

$$\int_{\boldsymbol{x}\in\Omega_x}\int_{\boldsymbol{\xi}\in\Omega_\xi}\boldsymbol{\xi}^{\boldsymbol{l}}\mathrm{F}^a(t,\boldsymbol{x};\boldsymbol{\xi})d^5\boldsymbol{\xi}d^3\boldsymbol{x}=\int_{\boldsymbol{x}\in\Omega_x}\int_{\boldsymbol{\xi}\in\Omega_\xi}\boldsymbol{\xi}^{\boldsymbol{l}}F(t,\boldsymbol{x};\boldsymbol{\xi})d^5\boldsymbol{\xi}d^3\boldsymbol{x} \tag{37}$$

where $\boldsymbol{l}\in\{0,1\}^5,\ l_1+\cdots+l_5\leq 1$ and $\boldsymbol{\xi}=\{\boldsymbol{\xi}_1,\ldots,\boldsymbol{\xi}_5\}$,

B. the new ASDF can be related to the discrete SDF, when the flow is made of a dilute disperse phase, such that the larger particle diameter is smaller than the inter-particle distance. We express this relation for a volume space $E\subset\Omega_x$, where the border of the domain does not cross any particle, as follows:

$$\int_{\boldsymbol{x}\in E}\mathrm{F}^a(t,\boldsymbol{x};\boldsymbol{\xi})d^3\boldsymbol{x}=\int_{\boldsymbol{x}\in E}F^d(t,\boldsymbol{x};\boldsymbol{\xi})d^3\boldsymbol{x}. \tag{38}$$

We recall that property A ensures the possibility to express the expected-mean interfacial quantities $(\Sigma(t,\boldsymbol{x}),\widetilde{H}(t,\boldsymbol{x}),\widetilde{G}(t,\boldsymbol{x}))$ as moments of the ASDF. Thanks to B, we can relate the ASDF to the NDF of the particles in the same way as in section 3.2.

We propose to define the averaged phase variables as follows:

$$\widetilde{\boldsymbol{\xi}}(t,\boldsymbol{x})=\int_{\boldsymbol{y}\in\Omega_x}w(\boldsymbol{x};\boldsymbol{y}-\boldsymbol{x})\,\delta_I(t,\boldsymbol{y})\boldsymbol{\xi}(t,\boldsymbol{y})d^3\boldsymbol{y}, \tag{39}$$

where $w(\boldsymbol{x};\boldsymbol{r}=\boldsymbol{y}-\boldsymbol{x})$ is a convolution kernel. The function $w(\boldsymbol{x};\boldsymbol{r})$ is chosen such that it vanishes for large $\|\boldsymbol{r}\|>h$, where $h>0$ is a characteristic spatial length scale, independent from the position $\boldsymbol{x}$. We now wish to design the kernel function so as to satisfy requirements A and B.

We can show that equation (37) of the first requirement A is verified under the sufficient condition:

$$\forall\boldsymbol{y}\in\Omega_x,\quad\int_{\boldsymbol{x}\in\Omega_x}w(\boldsymbol{x},\boldsymbol{y}-\boldsymbol{x})\delta_I(t,\boldsymbol{x})d^3\boldsymbol{x}=1. \tag{40}$$

Also, in order to fulfill the second requirement property B we look for a spatial-average of the interfacial variables (39) that degenerates to the interfacial average over one particle surface (23), when the inter-particle distance is much larger than the particles diameters. Hence, we choose a characteristic length scale h greater than the largest particle diameter and smaller than the inter-particle distance. Then we propose to use the following kernel function, which satisfies the condition (40):

$$w(\boldsymbol{x};\boldsymbol{r})=\frac{\mathbb{1}_{\|\boldsymbol{r}\|<h}(\boldsymbol{r})}{\int_{\boldsymbol{x}'\in\mathcal{V}_h(\boldsymbol{x}+\boldsymbol{r})}\delta_I(\boldsymbol{x}')d^3\boldsymbol{x}'}, \tag{41}$$

where $\mathcal{V}_h(\boldsymbol{x})=\{\boldsymbol{y}\in\Omega_x;\ \|\boldsymbol{x}-\boldsymbol{y}\|<h\}$. Therefore, $w(\boldsymbol{x},\boldsymbol{r})$ represents the inverse of the surface area included in $\mathcal{V}_h(\boldsymbol{x}+\boldsymbol{r})$. In the case where the volume $\mathcal{V}_h(\boldsymbol{x}+\boldsymbol{r})$ contains no interface, $w(\boldsymbol{x},\boldsymbol{r})$ is simply set to zero. This does not affect the definition of the averaged SDF.

4.2. Application for the construction of a NDF of deformed particles

We consider a space volume $E \subset \Omega_x$, containing a dispersed and dilute phase made of $N_{\max}$ droplets, $p_k,\ k = 1, \ldots, N_{\max}$ whose external boundaries are denoted by $\Sigma_k,\ k = 1, \ldots, N_{\max}$ and their center of mass by $\boldsymbol{x}_k,\ k = 1, \ldots, N_{\max}$. Let us note d_{max} the maximum diameter of these droplets. We moreover assume that the distance between droplets is larger than d_{max}. Let us note l_{min} the smallest distance between droplets. By considering a sufficiently large averaging scale h, $h > d_{max}$ (for example larger than the particle diameter so that each object is fully encompassed in the averaging process and its neighbors are not), one can ensure that the averaged Gauss curvature G is positive.

Using the averaged SDF defined in the previous section, we can define the following distribution function:

Definition The Generalized Number Density Function (GNDF) is defined as follows:

$$f_\Sigma(t, \boldsymbol{x}; \boldsymbol{\xi}) = \frac{G}{4\pi} \mathrm{F}^a(t, \boldsymbol{x}; \boldsymbol{\xi}). \tag{42}$$

Proposition 4.1. *If E is a space volume whose borders do not cross any particle, and* $l_{min} > h > d_{max}$*, then the integrals over E of the GNDF* $f_\Sigma(t, \boldsymbol{x}; \boldsymbol{\xi}) = \frac{G}{4\pi} \mathrm{F}^a(t, \boldsymbol{x}; \boldsymbol{\xi})$ *and the NDF* $f(t, \boldsymbol{x}; \boldsymbol{\xi})$ *are equal:*

$$\int\limits_{\boldsymbol{x} \in E} f_\Sigma(t, \boldsymbol{x}; \boldsymbol{\xi}) d^3\boldsymbol{x} = \int_{\boldsymbol{x} \in E} f(t, \boldsymbol{x}; \boldsymbol{\xi}) d^3\boldsymbol{x}. \tag{43}$$

Proof:. We can relate the averaged SDF F^a and the discrete SDF F^d as written in (38). Therefore, using equation (38), then from proposition 3.2, we have

$$\begin{aligned} 4\pi \int\limits_{\boldsymbol{x} \in E} f_\Sigma(t, \boldsymbol{x}; \boldsymbol{\xi}) d^3\boldsymbol{x} &= G \int\limits_{\boldsymbol{x} \in E} \mathrm{F}^a(t, \boldsymbol{x}; \boldsymbol{\xi}) d^3\boldsymbol{x} \\ &= G \int\limits_{\boldsymbol{x} \in E} F^d(t, \boldsymbol{x}; \boldsymbol{\xi}) d^3\boldsymbol{x} \\ &= 4\pi \int\limits_{\boldsymbol{x} \in E} f(t, \boldsymbol{x}; \boldsymbol{\xi}) d^3\boldsymbol{x} \end{aligned} \tag{44}$$

□

To conclude, the ASDF is related to a NDF (the GNDF) and can thus be used to describe statistically a dispersed flow of deformed droplets. Moreover we can derive the GPBE satisfied by the GNDF as in section 3.1:

$$\partial_t f_\Sigma + \nabla_{\boldsymbol{x}} \cdot \{\boldsymbol{V}_I f_\Sigma\} + \nabla_{\boldsymbol{\xi}} \cdot \{< \dot{\boldsymbol{\xi}} >_c f_\Sigma\} =< \Gamma >_c f_\Sigma, \tag{45}$$

where $\Gamma = \dot{\mathcal{S}} + \frac{\dot{G}}{G}$ is a source term of topology variation, mainly related to the breakup and coalescence phenomena. Thanks to the algorithms presented in the next section applied to DNS computations, we think it will be possible to propose modeling closures for the equation (45).

The theoretical framework considered in this section is restricted to dispersed and dilute phase. However, it seems that the SDF and the NDF are strongly related. The SDF can be seen as the origin of the NDF as discussed in [46]. The difficulty will to choose a length h that separates scales in the dense or separated flow regimes.

5. Algorithms and techniques for the numerical computation of the curvatures and of the SDF

In this section, we apply the results of the previous section to the design of a new numerical tool dedicated to the post-processing of DNS two-phase flows simulations. Such tool allows to enhance the analysis of the gas-liquid interface evolution. The DNS computations are performed using the ARCHER code [4], where a combined VOF and level-set approach is used to capture the interface, and a ghost method is applied to represent accurately the jump of variables across the liquid-gas interface.

Some numerical tools to compute the curvatures and the surface area of the gas-liquid interface present in each cell are already available in the ARCHER code [46]. Unfortunately, these quantities being computed separately, the Gauss-Bonnet formula can not be numerically satisfied. For this reason, we choose to compute the curvatures and the surface element areas by using the algorithm presented thereafter. Such algorithm will allow to obtain the number density function of droplets in DNS simulations, by using simple computations on the surface and without the need of an algorithm that isolates the droplets [47].

The new algorithm is implemented independently from the ARCHER code, from which only the distance function (Level-Set) data is used. The different algorithm steps are summarized as follows:

- The gas-liquid interface is discretized with a 2D triangulated mesh using the Marching Cubes algorithm [41]. This algorithm takes the $3D$ level-set scalar field as an input and returns a 2D meshed surface. This mesh is described with two arrays: the array of vertices, $\mathbf{V}$ of dimension $n_v \times 3$, and the array of faces (defined by three vertices), $\mathbf{F}$ of dimension $n_f \times 3$ which defines the connectivity between vertices. In this work, we use the Python package sckimage [48] to triangulate the surface.

- For each vertex $\mathrm{V} \in [1, n_v]$, $\mathbf{O}(\mathrm{V})$ denotes the set of neighbors of V: V' is a neighbor of V if both vertices share a same face $\mathrm{T} \in [1, n_f]$. By abuse of notation, $\mathbf{O}(\mathrm{V})$ also denotes the set of faces V belongs to and for each $\mathrm{T} \in \mathbf{O}(\mathrm{V})$, $\boldsymbol{N}(\mathrm{T})$ denotes the normal vector to the face, oriented toward the gas phase.

- In the neighborhood of V, we define its dual cell $\mathcal{M}(\mathrm{V})$ as a mix between the Voronoï cell (Figure 2b) and the barycentric cell (Figure 2a) around V, as proposed in [42]. Simply, for each triangular face T containing V, the Voronoï contour is considered if all the angle are acute. The barycentric contour is considered otherwise. Also, θ_{T} denotes the angle at vertex V in T, see Figure 2c, and $A[\mathrm{T}, \mathrm{V}] = \mathrm{area}(\mathrm{T} \cap \mathcal{M}(\mathrm{V}))$ is the area of the dual cell within the face T. Then, the discrete local surface area $A[\mathrm{V}]$, the normal $\boldsymbol{N}[\mathrm{V}]$ and the Gauss curvature

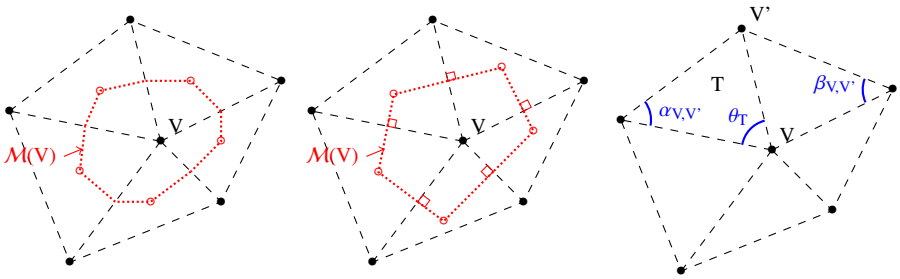

(a) $\mathcal{M}$(V) is a barycentric cell. (b) $\mathcal{M}$(V) is a Voronoï cell. (c) Illustration of angles.

Figure 2: Neighboring vertices and surface elements $\mathcal{M}$(V) around the vertex V.

G[V] can be computed:

$$A[\mathrm{V}] = \sum_{\mathrm{T}\in\mathbf{O}(\mathrm{V})} A[\mathrm{T},\mathrm{V}], \qquad \boldsymbol{N}[\mathrm{V}] = \frac{\sum\limits_{\mathrm{T}\in\mathbf{O}(\mathrm{V})} A[\mathrm{T},\mathrm{V}]\boldsymbol{N}(\mathrm{T})}{\left\| \sum\limits_{\mathrm{T}\in\mathbf{O}(\mathrm{V})} A[\mathrm{T},\mathrm{V}]\boldsymbol{N}(\mathrm{T}) \right\|},$$
$$G[\mathrm{V}] = \left(2\pi - \sum_{\mathrm{T}\in\mathbf{O}(\mathrm{V})} \theta_{\mathrm{T}}\right) / A[\mathrm{V}]. \tag{46}$$

- Finally, for each neighbour V′ of V, $\alpha_{\mathrm{V},\mathrm{V}'}$ and $\beta_{\mathrm{V},\mathrm{V}'}$ denote the two angles facing the edge [V, V′], without distinction, as illustrated in Figure 2c. Now, the local discrete mean curvature reads:

$$H[\mathrm{V}] = \frac{1}{2A[\mathrm{V}]} \sum_{\mathrm{V}'\in\mathbf{O}(\mathrm{V})} \left(\cot(\alpha_{\mathrm{V}',\mathrm{V}}) + \cot(\beta_{\mathrm{V}',\mathrm{V}})\right)\left(\mathbf{V}[\mathrm{V}] - \mathbf{V}[\mathrm{V}']\right)\cdot \boldsymbol{N}[\mathrm{V}]. \tag{47}$$

After computing the local geometrical quantities, we can evaluate the fine-grain localized SDF for one simulation, *i. e.* one realization. In the following, the phase space variables are restricted to the two curvatures $\boldsymbol{\xi} = (H, G) \in \Omega_{\xi}$: we do not consider the interface velocity. This 2D space is discretized into $n_h \times n_g$ phase-space cells $C_{i,j}$, such that the discrete phase space variables are expressed as follows:

$$\boldsymbol{\xi}_{i,j} = (H_i, G_j) = \boldsymbol{\xi}_{min} + (i\Delta H, j\Delta G), \quad (i,j) \in [1, n_h] \times [1, n_g],$$

where $\Delta H = (H_{max} - H_{min})/n_h$, $\Delta G = (G_{max} - G_{min})/n_g$ and the subscripts *min* and *max* refer respectively to the minimum and maximum values obtained by (46) and (47). The integral of the fine-grain localized SDF over a subdomain $E \subset \Omega_x$ can be approximated by:

$$\int_{\boldsymbol{x}\in E} F'(t, \boldsymbol{x}; \boldsymbol{\xi}_{i,j}) d^3\boldsymbol{x} \simeq \frac{1}{\Delta H \Delta G} \sum_{\mathrm{V}=1}^{n_v} A[\mathrm{V}]\, I_{C_{i,j}}(\boldsymbol{\xi}[\mathrm{V}])\, I_E(\mathbf{V}[\mathrm{V}]) \tag{48}$$

where $F'(t,\boldsymbol{x};\boldsymbol{\xi}_{i,j})$ is the fine-grain SDF defined in (15), $I_{C_{i,j}}(.)$ is the characteristic function of the cell $C_{i,j}$:

$$C_{i,j} = \{\boldsymbol{\xi}', |H' - H_{i,j}| \leq \Delta H/2 \text{ and } |G' - G_{i,j}| \leq \Delta G/2\},$$

and $I_E(.)$ is the characteristic function of the sub-domain E. In the following, we take $E = \Omega_x$. Thus the last equation becomes:

$$\int_{\boldsymbol{x}\in\Omega_x} F'(t,\boldsymbol{x};\boldsymbol{\xi}_{i,j})d^3\boldsymbol{x} \simeq \frac{1}{\Delta H\Delta G}\sum_{\mathrm{V}=1}^{n_v} A[\mathrm{V}]\, I_{C_{i,j}}(\boldsymbol{\xi}[\mathrm{V}]). \tag{49}$$

Using this numerical approximation, we define the numerical fine-grain SDF integrated in the whole domain as follows:

$$\mathcal{F}'(\boldsymbol{\xi}_{i,j}) = \frac{1}{\Delta H\Delta G}\sum_{\mathrm{V}=1}^{n_v} A[\mathrm{V}]\, I_{C_{i,j}}(\boldsymbol{\xi}[\mathrm{V}]). \tag{50}$$

To evaluate the averaged fine-grain SDF (36), we first calculate the averaged area and curvatures at each vertex $\mathrm{V} \in [1, n_v]$. These averaged quantities depend on the length scale h. In the following, we take $h = (k/2)\Delta x$, where Δx is the size of the level-set computation cells and $k \geq 1$ is an integer value to be set by the user. We denote by $\widetilde{A}^k[\mathrm{V}]$ and $\widetilde{\boldsymbol{\xi}}^k[\mathrm{V}]$ the numerical approximation of the averaged area and curvatures, defined in (39) and (41) and which are numerically evaluated as follows:

$$\begin{aligned} \widetilde{A}^k[\mathrm{V}] &= A[\mathrm{V}] \\ \widetilde{\boldsymbol{\xi}}^k[\mathrm{V}] &= \sum_{\mathrm{V}'\in\mathbf{O}_k(\mathrm{V})} \boldsymbol{\xi}[\mathrm{V}']\frac{A[\mathrm{V}']}{S_k[\mathrm{V}']}, \end{aligned} \tag{51}$$

where $\mathbf{O}_k(\mathrm{V})$ is the set of vertices V', such that $\|\mathbf{V}[\mathrm{V}] - \mathbf{V}[\mathrm{V}']\|_2 \leq k/2\Delta x$ and

$$S_k[\mathrm{V}'] = \sum_{\mathrm{V}''\in O_k(\mathrm{V}')} A(\mathrm{V}^{''}).$$

The numerical fine-grain averaged SDF is given by:

$$\mathcal{F}'^a(\boldsymbol{\xi}_{i,j}) = \frac{1}{\Delta H\Delta G}\sum_{\mathrm{V}=1}^{n_v} \widetilde{A}^k[\mathrm{V}] I_{C_{i,j}}(\widetilde{\boldsymbol{\xi}}^k[\mathrm{V}]). \tag{52}$$

Then, the numerical GNDF can be evaluated numerically as follows:

$$\mathcal{N}'(\boldsymbol{\xi}_{i,j}) = \frac{1}{\Delta H\Delta G}\sum_{\mathrm{V}=1}^{n_v} \frac{|\widetilde{G}^k[\mathrm{V}]|}{4\pi}\widetilde{A}^k[\mathrm{V}] I_{C_{i,j}}(\widetilde{\boldsymbol{\xi}}^k[\mathrm{V}]). \tag{53}$$

We recall that the spatial averaging of the curvatures and surface area distribution introduced in section 4.1, has been designed such that the first order moments of the SDF (37) are preserved. We can verify this property numerically as follows:

$$\begin{aligned} \int_{\Omega_x}\Sigma(t,\boldsymbol{x})d\boldsymbol{x} &\simeq \sum_{\mathrm{V}} A[\mathrm{V}] &&= \sum_{\mathrm{V}}\widetilde{A}^k[\mathrm{V}], \\ \int_{\Omega_x}\Sigma\widetilde{H}(t,\boldsymbol{x})d\boldsymbol{x} &\simeq \sum_{\mathrm{V}} H[\mathrm{V}]A[\mathrm{V}] &&= \sum_{\mathrm{V}}\widetilde{H}^k[\mathrm{V}]\widetilde{A}^k[\mathrm{V}], \\ \int_{\Omega_x}\Sigma\widetilde{G}(t,\boldsymbol{x})d\boldsymbol{x} &\simeq \sum_{\mathrm{V}} G[\mathrm{V}]A[\mathrm{V}] &&= \sum_{\mathrm{V}}\widetilde{G}^k[\mathrm{V}]\widetilde{A}^k[\mathrm{V}]. \end{aligned} \tag{54}$$

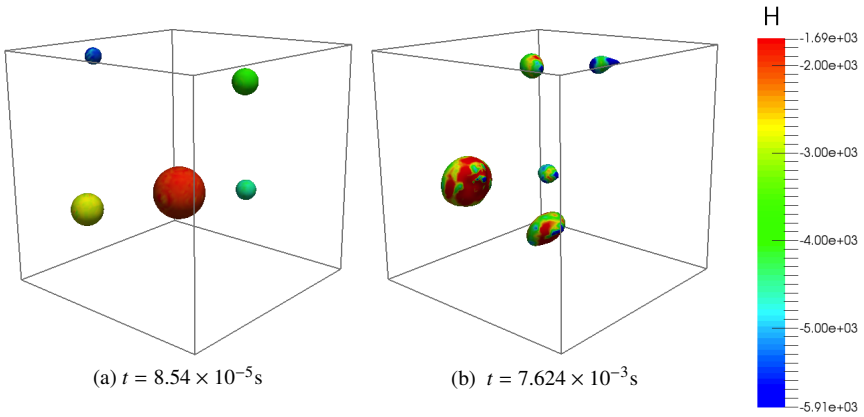

(a) $t = 8.54 \times 10^{-5}$s (b) $t = 7.624 \times 10^{-3}$s

Figure 3: Droplet surface colored according to the mean curvature values at the surfaces for two different times.

6. Assessment of the theoretical approach and DNS post-processing

In this section, we use the ARCHER code to perform some two-phase flows direct numerical simulations. The algorithms described in the previous section will be used to post-process the level-set data in order to compute the fine-grain SDF and NDF of a single simulation (one realization). Two numerical tests, with and without topological changes, allow to test the algorithm and the capacity to find some geometrical and topological feature of the gas-liquid interface, depending on a chosen averaging characteristic length-scale h defined in the previous section.

6.1. Droplets homeomorphic to spheres

In the first configuration, we consider five initial spherical water droplets of radii $r \in [0.33\text{ mm}, 1\text{ mm}]$ injected at a velocity 5 m/s in a 1 cm^3 periodic cubic domain of initially still gas. Classical water/air properties are used here. The initial positions of the droplet centers are chosen randomly, with the constraint however that the inter-droplet distance d_{drop} (computed from the droplet surface) is larger than $2r_{max}$, where initially $r_{max} = 1$ mm. The level-set function is represented in a grid of 96×96×96. Due to the difference between the gas and the droplet velocities, the shape of the droplets is deformed in time without break-up (the maximum Weber number is $We_{max} < 1$). In Figure 3, we display an illustration of the droplets at two successive times. The color indication at the droplet surfaces shows an estimate of the mean curvature. This first case is envisioned in the framework of no topological changes.

In Figure 4 (respectively 5), we plot the SDF for different averaged scales as a function of the Gauss (respectively the mean) curvature. The localized SDF, plotted with a blue line, corresponds to the length scale average $h = \Delta x/2$. In this case, the SDF is continuous and we can not identify the surface area contribution of each droplet. But, by using larger scales of average ($h = 25\Delta x/2$ and $h = 55\Delta x/2$), we see that we can identify five peaks which correspond to the five droplets. Indeed, when

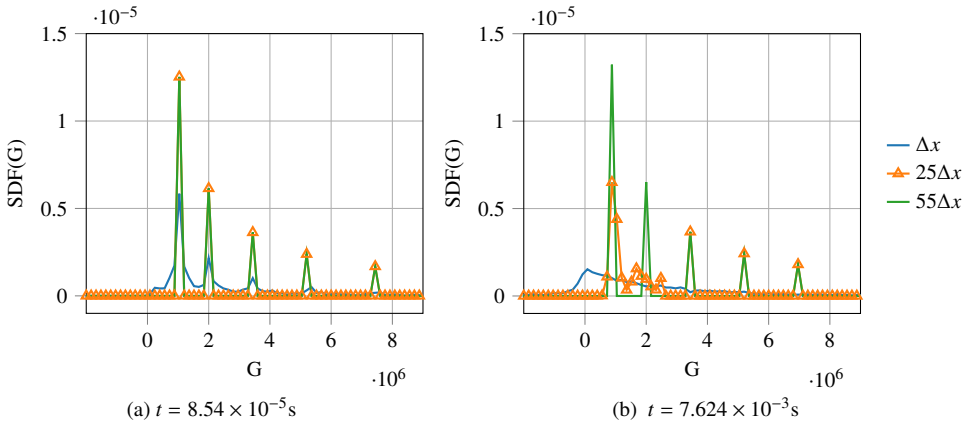

(a) $t = 8.54 \times 10^{-5}$s (b) $t = 7.624 \times 10^{-3}$s

Figure 4: Numerical SDF over the domain space as a function of the Gauss curvature: localized SDF (dashed-line), averaged SDF with $k = 25$ (triangle) and $k = 55$ (solid line).

$d_{drop} > h = 55\Delta x/2 > r_{max}$, for any point $\boldsymbol{x}$ situated at the interface of a droplet, the space volume $\mathcal{V}_h(\boldsymbol{x}) = \{\boldsymbol{y} \in \Omega_x;\ \|\boldsymbol{x}-\boldsymbol{y}\| < h\}$ contains that, and only that, droplet. Thus, for each droplet we compute one average mean and Gauss curvatures. Consequently, in this case the averaged SDF becomes a sum of Dirac delta function weighted by the surface area of the droplets.

In Figure 6 (respectively 7), we display the GNDF for different averaging scales. These distributions are obtained from the averaged SDFs using (53). When the averaging scale h is larger than the droplet diameters, we obtain five peaks of value 1. Then, we can count the right number of droplets for each averaged Gauss or mean curvature thanks to Gauss-Bonnet formula with a proper evaluation of the curvature and using our averaging approach. This assesses the proposed theoretical and algorithmic approach within the framework of no topological change.

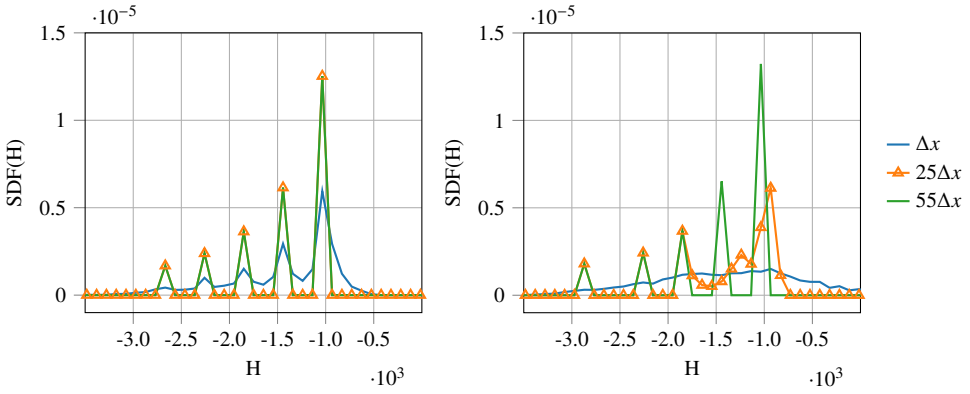

(a) $t = 8.54 \times 10^{-5}$s (b) $t = 7.624 \times 10^{-3}$s

Figure 5: Numerical SDF over the domain space as a function of the mean curvature: localized SDF (dashed-line), averaged SDF with $k = 25$ (triangle) and $k = 55$ (solid line).

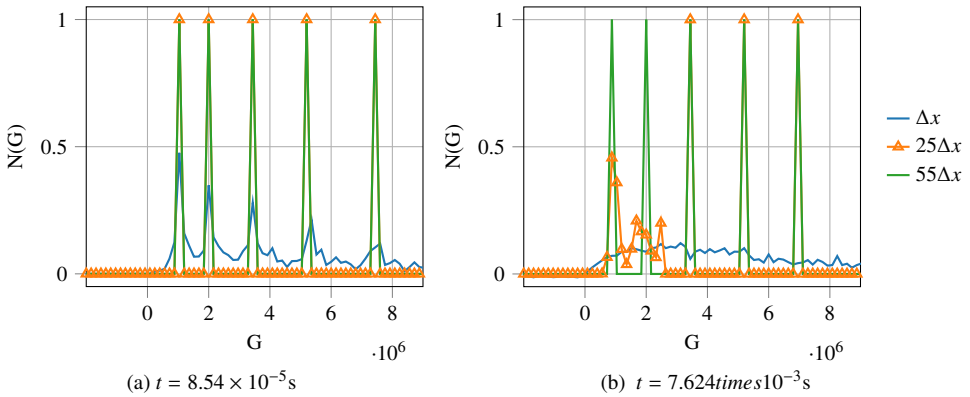

(a) $t = 8.54 \times 10^{-5}$s (b) $t = 7.624 times 10^{-3}$s

Figure 6: Numerical GNDF over the domain space as a function of the Gauss curvature: localized GNDF (dashed-line), averaged GNDF with $k = 25$ (triangle) and $k = 55$ (solid line).

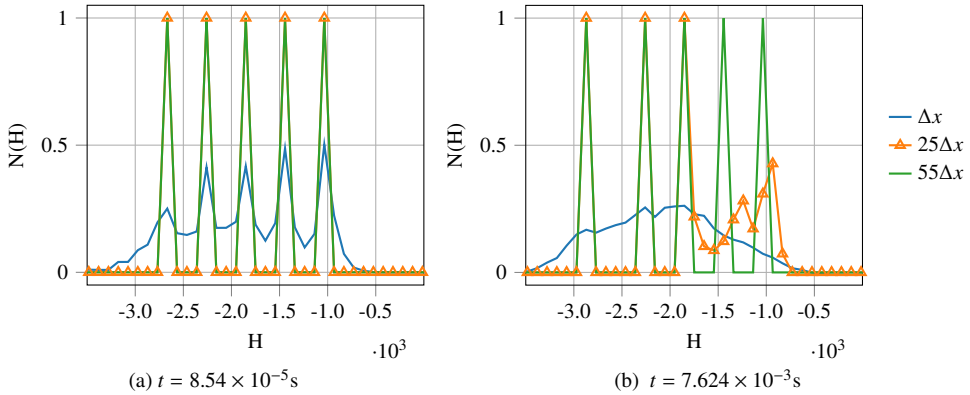

(a) $t = 8.54 \times 10^{-5}$s (b) $t = 7.624 \times 10^{-3}$s

Figure 7: Numerical GNDF over the domain space as a function of the mean curvature: localized GNDF (dashed-line), averaged GNDF with $k = 25$ (triangle) and $k = 55$ (solid line).

6.2. *Two droplets collision*

In this section, we consider a simulation of a two water droplets collision in the stretching separation regime [49]. The two droplets are initially separated (Figure 8a) in a periodic domain, with initial velocities. The collision leads to the temporary coalescence of the two droplets (Figure 8b) by forming a one unstable big droplet. Due to competition between inertial effect and surface tension, the unstable droplet deforms, first into a torus shape (Figure 8c) and finally breaks up into small different droplets (Figure 8d). The level-set function is represented in a grid of $64 \times 64 \times 128$.
The parameters of collision yield some important topological changes and are given in the following Table 1:

D_s (μm)	D_l (μm)	U_c ($m.s^{-1}$)	$We = \frac{\rho_l U_c D_s}{\sigma}$	x
260	400	4	60	0.42

Table 1: Parameters of droplet collision. Subscript s and l are related respectively to the small and large droplets. U_c is their relative velocity and x the dimensionless impact parameter [49]. Classical water and air properties are used.

In this simulation, we compute the time evolution of the volume integral over the whole computational domain of the zero and first order moments of the localized and averaged SDFs (Σ, $\Sigma\widetilde{H}$, $\Sigma\widetilde{G}$). We can see from Figures 9-11, that the moments of the averaged and localized SDF are equal at all time. This equality corresponds to the requirement A. The first two Figures 9-10 correspond respectively to the total surface area and the total mean curvature. These two quantities evolve continuously and we can identify from the two curves the different droplet states:

- $t \in [0, 2]$: the two droplets are initially separated,
- $t \in [2, 12]$: coalescence and stretching of the two droplets are characterized by a minimum total surface area at $t \in [3, 4]$, just after the coalescence. Then a

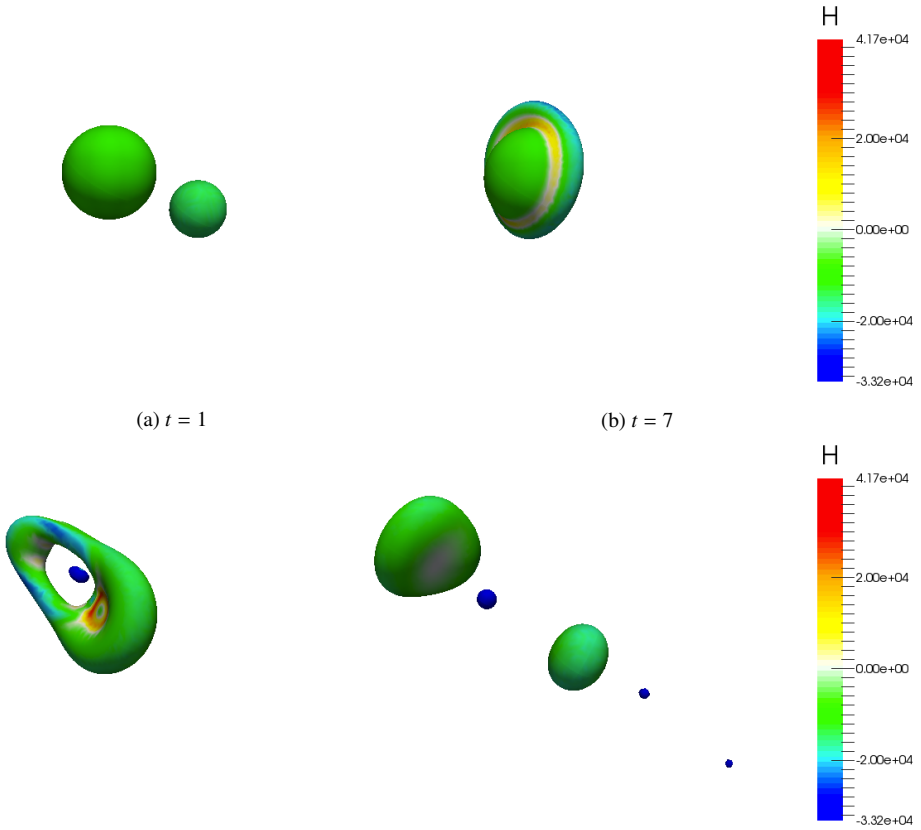

(a) $t = 1$ (b) $t = 7$

(c) $t = 14$ (d) $t = 60$

Figure 8: Simulation of collision and stretching separation of two droplets. Surface colored according to the local mean curvature (H) value.

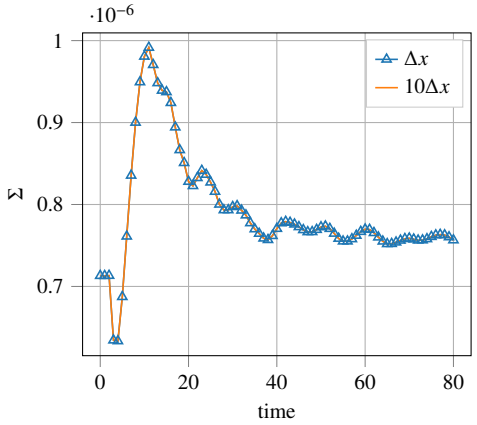

Figure 9: Time evolution of the total surface area $\int_{\boldsymbol{x}} \Sigma(\boldsymbol{x}) d\boldsymbol{x}$: without averaging (dashed-line), with scale average $k = 20$ (solid line).

maximum surface area is reached at $t \in [11, 12]$, just before the breakup occurs, when the thin liquid film reaches its maximum length. In the same time, we obtain a minimum of the absolute value of the total mean curvature. This can be explained by the positive values of mean curvature during coalescence.

- $t \in [12, 40]$: breakup cascade and coalescence of some small droplets take place. The total surface area decreases while the absolute value of the mean curvature increases,

- $t \in [40, 80]$: in the final state, we obtain five droplets, where we have a convergence of the total surface area and the total mean curvature toward stable values.

The evolution of total Gauss curvature illustrated in Figure 11 is discontinuous and by dividing this quantity by 4π, we obtain integer values. Indeed, the quantity $1/(4\pi) \int_{\boldsymbol{x}} \Sigma \widetilde{G} d\boldsymbol{x}$ is equal to the sum of the half of the Euler characteristic of the objects included in the entire domain. This quantity will allow us to evaluate the topology evolution. In the case of droplets homeomorphic to spheres, we get the droplets number in the domain. This is the case here with the exception of the period of time between time $t = 10$ and $t = 20$, where this quantity drops down from 1 to -2 and then increases to 0 and 1 before reaching 2 again, with two objects homeomorphic to a sphere. During this interval of time, the big droplet formed by the coalescence deforms into a torus shape with several holes and with satellite droplets and then we come back to a regular torus with another droplet homeomorphic to a sphere, that is a total characteristic of 1, before the torus closes, that is a characteristic of 2, and then breaks into a total of three droplets at time 20.

Thus, the proposed approach not only can lead to a statistics of objects through spatial averaging, when the whole set of objects are homeomorphic to spheres, but also provides some key informations about the topology of the interface.

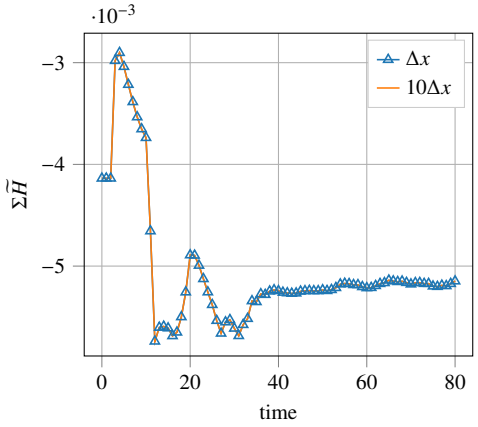

Figure 10: Time evolution of the total mean curvature $\int_{\boldsymbol{x}} \Sigma\widetilde{H}(\boldsymbol{x})d\boldsymbol{x}$: without averaging (dashed-line), with scale average $k = 20$ (solid line).

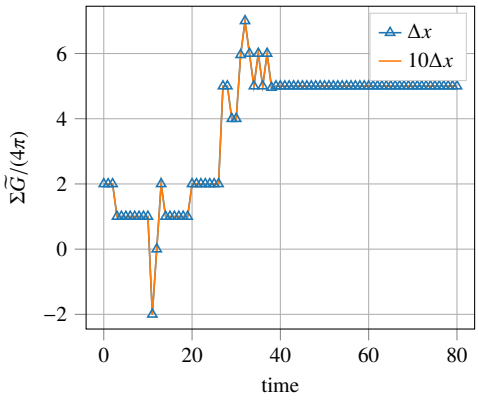

Figure 11: Time evolution of the total gauss curvature $\int_{\boldsymbol{x}} \Sigma\widetilde{G}(\boldsymbol{x})d\boldsymbol{x}$: without averaging (dashed-line), with scale average $k = 20$ (solid line).

7. Conclusion

In this paper, we have proposed a new statistical approach of the gas-liquid interface dedicated to two-phase flow modeling based on geometrical interface variables.

Relying on a statistical description of the interface between the two phases, our first contribution has been to propose a transport equation for a surface density function valid for both regimes: disperse and separated phases. The related phase space has been identified: it includes the curvatures and the velocity of the interface. An original link between such a surface density function formalism and its application to obtain statistics at the level of objects, such as the number density function (NDF) for sprays of droplets, has been proposed by introducing the discrete SDF (DSDF). The DSDF is only valid for disperse phase and supposes that we can isolate droplets/bubbles in small volumes. However, we can then describe droplets and bubbles with arbitrary shapes as long as they are homeomorphic to a sphere and this provides us with an interesting theoretical framework, which naturally degenerates to previous contributions when the objects are spherical [15].

In a second main contribution, we have defined the spatially averaged SDF (ASDF), with an averaging kernel bounded to a small region around the interface and which preserves some information of the standard SDF given by the first moments of this distribution. We have shown that the ASDF degenerates to the DSDF, when the liquid or gas phase is disperse. In this case, the link with the NDF can be identified straightforwardly and explicitly. We have then shown how we can derive reduced-order models from an equation on the SDF using the moments of these distributions. However, we still need a closure modeling in situations of complex topological changes, while we have illustrated that in some simplified situations (spherical droplets), a closure model can be derived [15, 40]. This model has already been used to simulate evaporating polydisperse sprays with variables related to interface geometry.

Finally, to illustrate and assess the theoretical part, we have designed a new algorithm to extract the curvatures and the two different distributions NDF and SDF from a level-set field obtained with the DNS ARCHER code. This new algorithm preserves some geometrical and topological information, which essentially allows us to compute a NDF from an ASDF. This new tool can serve, in a future work, to post-process more representative two-phase flows DNS simulations [46], with and without topological changes, and thus propose closure modeling of the curvatures evolutions and possibly closure of the distribution from its moments.

Acknowledgments

This research was supported by a Ph.D. grant for M. Essadki from IFP Energies Nouvelles. The support of Ecole Doctorale de Mathématiques Hadamard (EDMH) and EM2C Laboratory are gratefully acknowledged. This research was also supported by a Ph.D. grant for F. Drui from CEA/DGA at Maison de la Simulation and EM2C Laboratory. The support of ANR project "Mobilité durable et systèmes de transport (DS0603) - 2014" entitled "SUB SUPER JET : Modélisation de l'atomisation d'un jet liquide avec transition sous- et super-critique" (ANR-14-CE22-0014 - PI T. Schmitt) is also gratefully acknowledged. We would like to express our special thanks to our

colleagues from CORIA laboratory: R. Canu, F.X. Demoulin, B. Duret, S. Puggelli and J. Réveillon, and to our colleague from LJK: B. Thibert, for the numerous interesting and helpful discussions. The very helpful comments of S. Kokh and R. Di Battista are eventually gratefully acknowledged.

AppendixA. Evolution equation for the area density measure

In this section, let us derive the evolution equation for the area density measure δ_I. First, let us recall that δ_I is defined as a distribution function by:

$$\delta_I(t,\boldsymbol{x}) = \|\boldsymbol{\nabla}_{\boldsymbol{x}} g(t,\boldsymbol{x})\|\, \delta(g(t,\boldsymbol{x})).$$

The Lagrangian derivative $\dot{\bullet}$ of δ_I reads:

$$\begin{aligned}\dot{\delta}_I(t,\boldsymbol{x}) &= \partial_t \delta_I + \boldsymbol{V}_I \cdot \boldsymbol{\nabla}_{\boldsymbol{x}} \delta_I \\ &= \left[\partial_t \left(\|\boldsymbol{\nabla}_{\boldsymbol{x}} g(t,\boldsymbol{x})\|\right) + \boldsymbol{V}_I \cdot \boldsymbol{\nabla}_{\boldsymbol{x}} (\|\boldsymbol{\nabla}_{\boldsymbol{x}} g(t,\boldsymbol{x})\|)\right] \delta(g(t,\boldsymbol{x})) \\ &\quad + \left[\partial_t \left(\delta(g(t,\boldsymbol{x}))\right) + \boldsymbol{V}_I \cdot \boldsymbol{\nabla}_{\boldsymbol{x}} (\delta(g(t,\boldsymbol{x})))\right] \|\boldsymbol{\nabla}_{\boldsymbol{x}} g(t,\boldsymbol{x})\|\end{aligned}$$

The second term in the right-hand side of the previous equality is null, because of the equation on $g(t,\boldsymbol{x})$ which is:

$$\partial_t g + \boldsymbol{V}_I \cdot \boldsymbol{\nabla}_{\boldsymbol{x}} g = 0.$$

Let us now compute the first term. On a one hand, we have:

$$\begin{aligned}\partial_t \left(\|\boldsymbol{\nabla}_{\boldsymbol{x}} g(t,\boldsymbol{x})\|\right) &= \frac{\boldsymbol{\nabla}_{\boldsymbol{x}} g(t,\boldsymbol{x})}{\|\boldsymbol{\nabla}_{\boldsymbol{x}} g(t,\boldsymbol{x})\|} \cdot \partial_t \left(\boldsymbol{\nabla}_{\boldsymbol{x}} g(t,\boldsymbol{x})\right) \\ &= \boldsymbol{N} \cdot \boldsymbol{\nabla}_{\boldsymbol{x}} (\partial_t g(t,\boldsymbol{x})) \\ &= -\boldsymbol{N} \cdot \boldsymbol{\nabla}_{\boldsymbol{x}} (\boldsymbol{V}_I \cdot \boldsymbol{\nabla}_{\boldsymbol{x}} g(t,\boldsymbol{x})) \\ &= -\boldsymbol{N} \cdot \boldsymbol{\nabla}_{\boldsymbol{x}} (V_I \|\boldsymbol{\nabla}_{\boldsymbol{x}} g(t,\boldsymbol{x})\|).\end{aligned}$$

On the other hand, one computes:

$$\begin{aligned}\boldsymbol{V}_I \cdot \boldsymbol{\nabla}_{\boldsymbol{x}} (\|\boldsymbol{\nabla}_{\boldsymbol{x}} g(t,\boldsymbol{x})\|) &= V_I \boldsymbol{N} \cdot \boldsymbol{\nabla}_{\boldsymbol{x}} (\|\boldsymbol{\nabla}_{\boldsymbol{x}} g(t,\boldsymbol{x})\|) \\ &= \boldsymbol{N} \cdot \boldsymbol{\nabla}_{\boldsymbol{x}} (V_I \|\boldsymbol{\nabla}_{\boldsymbol{x}} g(t,\boldsymbol{x})\|) - \|\boldsymbol{\nabla}_{\boldsymbol{x}} g(t,\boldsymbol{x})\| \boldsymbol{N} \cdot \boldsymbol{\nabla}_{\boldsymbol{x}} (V_I)\end{aligned}$$

And finally, one can find that:

$$\begin{aligned}\dot{\delta}_I(t,\boldsymbol{x}) &= -\|\boldsymbol{\nabla}_{\boldsymbol{x}} g(t,\boldsymbol{x})\| \boldsymbol{N} \cdot \boldsymbol{\nabla}_{\boldsymbol{x}} (V_I)\, \delta(g(t,\boldsymbol{x})) \\ &= -\delta_I\, \boldsymbol{N} \cdot \boldsymbol{\nabla}_{\boldsymbol{x}} (V_I). \end{aligned} \tag{A.1}$$

Equation (A.1) can be further developed, by noting that:

$$-\delta_I\, \boldsymbol{N} \cdot \boldsymbol{\nabla}_{\boldsymbol{x}} (V_I) = -\delta_I\, [\nabla_{\boldsymbol{x}} \cdot \boldsymbol{V}_I - V_I \nabla_{\boldsymbol{x}} \cdot \boldsymbol{N}]$$

and

$$\nabla_{\boldsymbol{x}} \cdot \boldsymbol{N} = 2H.$$

Finally, one has:

$$\dot{\delta}_I(t,\boldsymbol{x}) = -\delta_I\, \nabla_{\boldsymbol{x}} \cdot \boldsymbol{V}_I + 2H \delta_I V_I. \tag{A.2}$$

AppendixB. Spray modeling framework

In this section, we focus on the simplified case of an evaporating spray, which consists in a cloud of polydiserse and spherical droplets. We also suppose that the spray is dilute enough and the Weber number low enough, so that coalescence and fragmentation of the droplets can be neglected. Such configuration occurs downstream the fuel injection in direct injection engines. Finally, for the sake of simplicity and clarity, we assume that thermal transfer can also be neglected, so that the temperature of the droplets can be ignored[2]. Under the hypothesis that the droplets stay spherical at all times, the NDF writes:

$$f(t,\boldsymbol{x};H,G,\boldsymbol{V}_I) = N(t,\boldsymbol{x};S=4\pi/G,\boldsymbol{V}_I)\,\delta(H-\mathsf{H}(S)) \tag{B.1}$$

where the mean curvature, $\mathsf{H}(S) = \sqrt{4\pi/S}$ is function of the surface S. Therefore, we can reduce the phase-space variables to the surface area S and the averaged interface velocity $\boldsymbol{V}_I$. Let us also note that under additional assumptions of incompressibility of the droplet and of a uniform evaporation at the droplet surface, $\boldsymbol{V}_I$ is now equal to $\boldsymbol{V}_p$, the velocity of the center of mass of the droplet. In the following, we consider dimensionless variables, so that the surface area $S \in [0,1]$. The GPBE equation satisfied by the new NDF, $N(t,\boldsymbol{x};S,\boldsymbol{V}_p)$ can be derived from (35):

$$\partial_t N + \nabla_{\boldsymbol{x}}\cdot\{\boldsymbol{V}_p N\} + \nabla_{\boldsymbol{V}_p}\cdot\{\dot{\boldsymbol{V}}_p N\} + \partial_S\{\dot{S}N\} = 0. \tag{B.2}$$

The droplet acceleration $\dot{\boldsymbol{V}}_p$ is equal to the sum of forces per unit of mass acting on the droplet. In the following, we consider that the only force acting on the droplets is the drag due to the carrier gas. This can be modeled in a first time by a linear Stokes law:

$$\dot{\boldsymbol{V}}_p = \frac{\boldsymbol{U}_g - \boldsymbol{V}_p}{\mathrm{St}(S)}, \tag{B.3}$$

where $\mathrm{St}(S) = \theta S$ is the Stokes number, which depends linearly on the surface area S. The coefficient θ depends on the physical properties of the gas and the liquid.

Since we consider spherical and non-deforming droplets, the evolution of the surface area is only due to evaporation. The Lagrangian-time derivative of the surface area is equal to the evaporation:

$$\dot{S} = \mathrm{R}_S(S). \tag{B.4}$$

Assuming a d^2 law for the phenomenon, the evaporation rate is constant: $\mathrm{R}_S(S) = -\mathrm{K}$.

Finally, the NDF satisfies the following simplified and dimensionless form of the Williams-Boltzmann Equation (WBE) [13]:

$$\partial_t N + \nabla_{\boldsymbol{x}}\cdot\{\boldsymbol{V}_p N\} = -\nabla_{\boldsymbol{V}_p}\cdot\left\{\frac{\boldsymbol{U}_g - \boldsymbol{V}_p}{\theta S}N\right\} + \mathrm{K}\partial_S\{N\}. \tag{B.5}$$

Here, we would like to emphasize the fact that this equation is well known in statistical modeling of the spray and has been derived here from a statistical gas-liquid interface approach.

[2]This assumption is merely made in order to simplify the exposition since we know that we have to deal with the temperature when evaporation/combustion is present [50, 23, 51].

Here again, the high-dimensional nature of the phase-space of the WBE makes its discretization unreachable for complex industrial applications within a reasonable CPU time. Since the exact NDF is not required and only macroscopic quantities of the flows are needed, an Eulerian moment method can be used to reduce its complexity. The derivation of a system of equations for the evolution of a set of some NDF moments often involves other moments of lower or higher order or even other terms which depend on the NDF. Therefore, we need to propose a closure for the size and velocity distributions. This closure step depends on the considered moments used to describe the spray. The set of moments and their order are chosen depending on the application and the desired accuracy to capture some specific spray feature: for example, the droplet segregation or the polydispersion effect on the evaporation [52, 53, 17].

First, we close the NDF in the velocity direction. The main issue in modeling the velocity distribution in an Eulerian framework is the particle trajectory crossing (PTC), occurring especially for inertial droplets [54, 52]. For accurate modeling of the PTC, one could use high order velocity-moment closure, such as the anisotropic Gaussian velocity distribution [54, 52]. In the present work, we consider a simplified model based on a monokinetic assumption [19]:

$$N(t,\boldsymbol{x};S,\boldsymbol{V}_p) = n(t,\boldsymbol{x},S)\,\delta(\boldsymbol{V}_p - \boldsymbol{U}_p(t,\boldsymbol{x})), \tag{B.6}$$

so that at a given point in space and time, all the particles have the same velocity. This assumption is valid for low inertia droplets ($\mathrm{St}(S) < 1$), when the droplet velocities are rapidly relaxed to the local gas velocity and droplets do not experience too much crossing. Then, from equation (B.2), by considering the two first moments in velocity, we derive the following semi-kinetic equation:

$$\begin{aligned} \partial_t n + \partial_{\boldsymbol{x}}\cdot\left(n\boldsymbol{U}_p\right) &= \mathrm{K}\,\partial_S n, \\ \partial_t n\boldsymbol{U} + \partial_{\boldsymbol{x}}\cdot\left(n\boldsymbol{U}_p\otimes\boldsymbol{U}_p\right) &= \mathrm{K}\,\partial_S\left(n\boldsymbol{U}_p\right) + n\frac{\boldsymbol{U}_g-\boldsymbol{U}_p}{\mathrm{St}(S)}. \end{aligned} \tag{B.7}$$

This system describes the time evolution of the size distribution $n(t,\boldsymbol{x},S)$ due to the transport in the physical space and evaporation and drag source terms.

AppendixB.1. Fractional size moments and relation to the interface average geometry

In the case of spherical droplets, the averaged interfacial quantities (surface area density and Gauss and mean curvatures), that have been expressed as moments of the NDF $f(t,\boldsymbol{x};H,S,v,\boldsymbol{V}_I)$ in equations (19), can now be expressed as moments of the simplified NDF $n(t,\boldsymbol{x},S)$ as follows:

$$\begin{aligned} \Sigma_d\widetilde{G}_d &= 4\pi\mathrm{m}_0, \\ \Sigma_d\widetilde{\mathrm{H}}_d &= 2\sqrt{\pi}\mathrm{m}_{1/2}, \\ \Sigma_d &= \mathrm{m}_1, \\ \alpha_d &= \frac{1}{6\sqrt{\pi}}\mathrm{m}_{3/2}, \end{aligned} \tag{B.8}$$

where a fractional size-moment is given by:

$$\mathrm{m}_{k/2}(t,\boldsymbol{x}) = \int_0^1 S^{k/2} n(t,\boldsymbol{x},S)dS. \tag{B.9}$$

Now, from the semi-kinetic equation (B.7) we derive a high order fractional moment model. This model gives the evolution of the mean geometrical interfacial variables for spherical and polydisperse droplets, involving transport, evaporation and drag force:

$$\begin{cases} \partial_t \mathrm{m}_0 & + & \partial_{\boldsymbol{x}} \cdot \left(\mathrm{m}_0 \boldsymbol{U}_p\right) & = & -\mathrm{K} n(t, \boldsymbol{x}, S=0), \\ \partial_t \mathrm{m}_{1/2} & + & \partial_{\boldsymbol{x}} \cdot \left(\mathrm{m}_{1/2} \boldsymbol{U}_p\right) & = & -\dfrac{\mathrm{K}}{2} \mathrm{m}_{-1/2}, \\ \partial_t \mathrm{m}_1 & + & \partial_{\boldsymbol{x}} \cdot \left(\mathrm{m}_1 \boldsymbol{U}_p\right) & = & -\mathrm{K} \mathrm{m}_0, \\ \partial_t \mathrm{m}_{3/2} & + & \partial_{\boldsymbol{x}} \cdot \left(\mathrm{m}_{3/2} \boldsymbol{U}_p\right) & = & -\dfrac{3\mathrm{K}}{2} \mathrm{m}_{1/2}, \\ \partial_t \left(\mathrm{m}_1 \boldsymbol{U}\right) & + & \partial_{\boldsymbol{x}} \cdot \left(\mathrm{m}_1 \boldsymbol{U}_p \otimes \boldsymbol{U}_p\right) & = & -\mathrm{K} \mathrm{m}_0 \boldsymbol{U}_p + \mathrm{m}_0 \dfrac{\boldsymbol{U}_g - \boldsymbol{U}_p}{\theta}, \end{cases} \tag{B.10}$$

where the pointwise disappearance flux $-\mathrm{K} n(t, \boldsymbol{x}, S=0)$ at size zero and the negative order moment $\mathrm{m}_{-1/2} = \int_0^1 S^{-1/2} n(t,S) dS$ depend on the size distribution, which is an unknown function in this model.

AppendixB.2. Closure relations for the fractional moments model

In the following, we use a smooth reconstruction of the size distribution through the maximisation of Shannon's entropy [25], in order to close the system of equations. This reconstruction has been already used in [24, 55] and shows a high capacity to model the polydispersion effect on the evaporation and the drag force response of droplets compared to the Multi-fluid approach [20, 23]. In the case of fractional moments (B.9), the reconstruction by entropy maximization reads:

$$\max \left\{ E_{sh}[n] = -\int_0^1 n(S) \ln(n(S)) dS \right\}, \quad \text{s. t.} \quad \mathrm{m}_{k/2} = \int_0^1 S^{k/2} n(S) dS, \; k = 0 \ldots N, \tag{B.11}$$

The existence and uniqueness of such a reconstruction have been proved in [15] and the reconstructed NDF has the following form:

$$n^{ME}(S) = \exp\left(-(\lambda_0 + \lambda_1 S^{1/2} + \lambda_2 S + \lambda_3 S^{3/2})\right). \tag{B.12}$$

To determine the λ_k coefficients, we use a similar algorithm as the one used for integer moment [25].

Fractional size moments can be seen as a first and simple model derived successfully from the statistical gas-liquid interface approach introduced in 3.1. In this model, we suppose the droplets to be spherical. This allows to obtain the system (B.10), which is closed by mean of a reconstructed size distribution through entropy maximization. In this case, droplet deformation is neglected and the evaporation is the only source term acting on the size variation. Yet, the actual model can be used for polydisperse evaporating sprays. In future work, it could be enriched by it coupling with a model for the gas-liquid interface.

The numerical resolution of system (B.10) may be achieved through an operator splitting algorithm [56, 57], that integrates independently the transport part (left-hand side of system (B.10)) and the source terms (right-hand side of system (B.10)). The

transport part is solved using a kinetic scheme [19] adapted for fractional moments. A new solver for the source terms (evaporation and drag force) is proposed in [15]. The proposed numerical schemes ensure the realizability of the moments and show a high accuracy for evaporation effects at 0D and 1D transport [15]. The new model was also compared to the EMSM model for a 2D evaporating case [15, 40]. Finally in [40], a 3D adaptive mesh refinement simulation compares droplet segregation with a Lagrangian simulation for non evaporating droplets in the presence of a frozen homogeneous isotropic turbulent gas.

References

[1] C. Hirt, B. Nichols, Volume of fluid (vof) method for the dynamics of free boundaries, Journal of Computational Physics 39 (1) (1981) 201–225.

[2] S. Osher, R. P. Fedkiw, Level set methods: An overview and some recent results, Journal of Computational Physics 169 (2) (2001) 463–502.

[3] A. Bourlioux, A coupled level-set volume-of-fluid algorithm for tracking material interfaces, in: Proceedings of the 6th International Symposium on Computational Fluid Dynamics, Lake Tahoe, CA, 1995.

[4] T. Menard, S. Tanguy, A. Berlemont, Coupling level set/VOF/ghost fluid methods: Validation and application to 3D simulation of the primary break-up of a liquid jet, International Journal of Multiphase Flow 33 (5) (2007) 510–524.

[5] C. Hirt, A. Amsden, J. Cook, An arbitrary lagrangian-eulerian computing method for all flow speeds, Journal of Computational Physics 14 (3) (1974) 227–253.

[6] R. Lebas, T. Menard, P. A. Beau, A. Berlemont, F. X. Demoulin, Numerical simulation of primary break-up and atomization: DNS and modelling study, International Journal of Multiphase Flows 35 (3) (2009) 247–260.

[7] O. Desjardins, J. McCaslin, M. Owkes, P. Brady, Direct numerical and large-eddy simulation of primary atomization in complex geometries, Atomization and Sprays 23 (11) (2013) 1001–1048.

[8] S. Ghods, M. Herrmann, A consistent rescaled momentum transport method for simulating large density ratio incompressible multiphase flows using level set methods, Physica Scripta 2013 (T155) (2013) 014050.

[9] V. Le Chenadec, H. Pitsch, A monotonicity preserving conservative sharp interface flow solver for high density ratio two-phase flows, J. Comput. Phys. 249 (2013) 185–203.

[10] G. Vaudor, T. Ménard, W. Aniszewski, M. Doring, A. Berlemont, A consistent mass and momentum flux computation method for two phase flows. application to atomization process, Computers & Fluids 152 (Supplement C) (2017) 204 – 216.

[11] D. Fuster, A. Bagué, T. Boeck, L. L. Moyne, A. Leboissetier, S. Popinet, P. Ray, R. Scardovelli, S. Zaleski, Simulation of primary atomization with an octree adaptive mesh refinement and vof method, International Journal of Multiphase Flow 35 (6) (2009) 550 – 565.

[12] Y. Ling, D. Fuster, S. Zaleski, G. Tryggvason, Spray formation in a quasiplanar gas-liquid mixing layer at moderate density ratios: A numerical closeup, Phys. Rev. Fluids 2 (2017) 014005.

[13] F. Williams, Spray combustion and atomization, Physics of Fluids 1 (1958) 541–545.

[14] G. A. Bird, Molecular gas dynamics and the direct simulation of gas flows, Oxford Science Publications 42.

[15] M. Essadki, S. de Chaisemartin, F. Laurent, M. Massot, High order moment model for polydisperse evaporating sprays towards interfacial geometry description, SIAM Journal on Applied Mathematics 78 (4) (2018) 2003–2027.

[16] A. Tagliani, Hausdorff moment problem and maximum entropy: a unified approach, Applied Mathematics and Computation 105 (1999) 291–305.

[17] A. Vié, S. Jay, B. Cuenot, M. Massot, Accounting for Polydispersion in the Eulerian Large Eddy Simulation of an Aeronautical-type Configuration, Flow Turbulence and Combustion 90 (3) (2013) 545–581.

[18] G. Hannebique, P. Sierra, E. Riber, B. Cuenot, Large Eddy Simulation of reactive two-phase flow in an aeronautical multipoint burner, Flow, Turbulence and Combustion 90 (2013) 449–469.

[19] S. de Chaisemartin, L. Fréret, D. Kah, F. Laurent, R. Fox, J. Reveillon, M. Massot, Eulerian models for turbulent spray combustion with polydispersity and droplet crossing, Comptes Rendus Mécanique 337 (2009) 438–448, special Issue 'Combustion for Aerospace Propulsion'.

[20] F. Laurent, A. Sibra, F. Doisneau, Two-size moment Eulerian multi-fluid model: a robust and high-fidelity description of polydisperse moderately dense evaporating sprays, Communications in Computational Physics 20 (2016) 902–943.

[21] T. T. Nguyen, F. Laurent, R. O. Fox, M. Massot, Solution of population balance equations in applications with fine particles: mathematical modeling and numerical schemes, Journal of Computational Physics 325 (2016) 129–156.

[22] C. Yuan, F. Laurent, R. Fox, An extended quadrature method of moments for population balance equations, Atomization and Sprays 51 (1) (2012) 1–23.

[23] O. Emre, D. Kah, S. Jay, Q.-H. Tran, A. Velghe, S. De Chaisemartin, F. Laurent, M. Massot, Eulerian Moment Methods for Automotive Sprays, Atomization and Sprays 25 (2015) 189–254.

[24] M. Massot, F. Laurent, D. Kah, S. de Chaisemartin, A robust moment method for evaluation of the disappearance rate of evaporating sprays, SIAM Journal on Applied Mathematics 70 (2010) 3203–3234.

[25] L. R. Mead, N. Papanicolaou, Maximum entropy in the problem of moments, Journal of Mathematical Physics 25 (8) (1984) 2404–2417.

[26] D. Kah, Taking into account polydispersity in the framework of a coupled euler-lagrange approach for the modeling of liquid fuel injection in internal combustion engines, Ph.D. thesis, Ecole Centrale Paris, available online at http://tel.archives-ouvertes.fr/tel-00618786/en/ (2010).

[27] G. Chanteperdrix, P. Villedieu, J. Vila, A compressible model for separated two-phase flows computations, in: ASME Fluids Engineering Division Summer Meeting, Montreal, 2002.

[28] A. Murrone, H. Guillard, A five equation reduced model for compressible two phase flow problems, Journal of Computational Physics 205 (2005) 664–698.

[29] A. Bernard-Champmartin, F. De Vuyst, A low diffusive lagrange-remap scheme for the simulation of violent air–water free-surface flows, Journal of Computational Physics 274 (2014) 19–49.

[30] M. Ishii, Thermo-Fluid dynamic theory of two-phase flow, Eyrolles, 1975.

[31] D. Drew, S. Passman, Theory of multicomponent fluids, Vol. 135, Springer, 1999.

[32] S. Gavrilyuk, R. Saurel, Mathematical and numerical modeling of two-phase compressible flows with micro-inertia, Journal of Computational Physics 175 (2002) 326–360.

[33] F. Drui, S. Kokh, A. Larat, M. Massot, Small-scale kinematics of two-phase flows: identifying relaxation processes in separated- and disperse-phase flow models, Journal of Fluid Mechanics 876 (2019) 326–355.

[34] C. Le Touze, Coupling between separated and dispersed two-phase flow models for the simulation of primary atomization in cryogenic combustion, Ph.D. thesis, Universite Nice Sophia Antipolis, available on TEL https://tel.archives-ouvertes.fr/tel-01250527 (Dec. 2015).

[35] A. Vallet, R. Borghi, Modélisation eulerienne de l'atomisation d'un jet liquide, Comptes Rendus de l'Académie des Sciences - Series IIB - Mechanics-Physics-Astronomy 327 (10) (1999) 1015 – 1020.

[36] A. Vallet, A. Burluka, R. Borghi, Development of a eulerian model for the "atomization" of a liquid jet, Atomization and Sprays 11 (2001) 619–642.

[37] M. B. Devassy, C. Habchi, D. E., Atomization modelling of liquid jets using a two-surface-density approach, Journal of Atomization and Sprays 25 (1) (2015) 47–80.

[38] D. A. Drew, Evolution of geometric statistics, SIAM Journal on Applied Mathematics 50 (3) (1990) 649–666.

[39] S. B. Pope, The evolution of surfaces in turbulence, Journal of Engineering Science 6 (5) (1988) 445–469.

[40] M. Essadki, S. de Chaisemartin, M. Massot, F. Laurent, A. Larat, S. Jay, High order moment methods and adaptive mesh refinement for polydisperse evaporating spray simulations, Oil & Gas Science and Technology 71 (2016) 1–25.

[41] L. Thomas, L. Hélio, V. Antônio Wilson, T. Geovan, Efficient implementation of marching cubes cases with topological guarantees, Journal of Graphics Tools 8 (2) (2003) 1–15.

[42] M. Meyer, M. Desbrun, P. Schröder, A. H. Barr, Discrete differential-geometry operators for triangulated 2-manifolds, in: Visualization and mathematics III, Springer, 2003, pp. 35–57.

[43] G. Kindlmann, R. Whitaker, T. Tasdizen, T. Moller, Curvature-based transfer functions for direct volume rendering : Methods and applications, in: Visualization, 2003., IEEE, 2003, pp. 513–520.

[44] C. Morel, Mathematical Modeling of Disperse Two-Phase Flows, Vol. 114, Springer International Publishing, 2015.

[45] E. Abbena, S. Salamon, A. Gray, Modern Differential Geometry of Curves and Surfaces with MATHEMATICA, CRC Press, 2006.

[46] R. Canu, S. Puggelli, M. Essadki, B. Duret, T. Menard, M. Massot, J. Reveillon, F. Demoulin, Where does the droplet size distribution come from?, International Journal of Multiphase Flow 107 (2018) 230 – 245.

[47] M. Kang, R. Fedkiw, X.-D. Liu, A boundary condition capturing method for multiphase incompressible flow, Journal of Scientific Computing 15 (3) (2000) 323–360.

[48] S. van der Walt, J. L. Schönberger, J. Nunez-Iglesias, F. Boulogne, J. D. Warner, N. Yager, E. Gouillart, T. a. Yu, scikit-image: image processing in python, PeerJ 2 (2014) e453.

[49] N. Ashgriz, J. Y. Poo, Coalescence and separation in binary collisions of liquid drops, Journal of Fluid Mechanics 221 (1990) 183–204.

[50] M. Massot, M. Kumar, A. Gomez, M. D. Smooke, Counterflow spray diffusion flames of heptane: computations and experiments, in: Proceedings of the 27th Symp. (International) on Combustion, The Comb. Institute, 1998, pp. 1975–1983.

[51] A. Sibra, J. Dupays, A. Murrone, F. Laurent, M. Massot, Simulation of reactive polydisperse sprays strongly coupled to unsteady flows in solid rocket motors: Efficient strategy using eulerian multi-fluid methods, Journal of Computational Physics 339 (2017) 210 – 246.

[52] M. Sabat, Eulerian modeling and numerical methods for the description of turbulent polydisperse sprays, Ph.D. thesis, Université Paris-Saclay, CentraleSupélec (2016).

[53] M. Sabat, A. Vié, A. Larat, M. Massot, Statistical description of turbulent particle-laden flows in the very dilute regime using the anisotropic gaussian moment method, International Journal of Multiphase Flow 112 (2019) 243 – 257.

[54] A. Vié, F. Doisneau, M. Massot, On the Anisotropic Gaussian closure for the prediction of inertial-particle laden flows, Communications in Computational Physics 17 (1) (2015) 1–46.

[55] D. Kah, O. Emre, Q. Tran, S. de Chaisemartin, S. Jay, F. Laurent, M. Massot, High order moment method for polydisperse evaporating spray with mesh movement: application to internal combustion engines, Int. J. Multiphase Flows 71 (2015) 38–65.

[56] F. Doisneau, A. Sibra, J. Dupays, A. Murrone, F. Laurent, M. Massot, Numerical strategy for unsteady two-way coupled polydisperse sprays: application to solid-rocket instabilities, Journal of Propulsion and Power, 3 (2014) 727–748.

[57] S. Descombes, M. Duarte, T. Dumont, F. Laurent, V. Louvet, M. Massot, Analysis of operator splitting in the non-asymptotic regime for nonlinear reaction-diffusion equations. application to the dynamics of premixed flames, SIAM Journal on Numerical Analysis 52 (2014) 1311–1334.